Sea Ice Climate Change Initiative: Phase 1

ANT D1.6 ICESat ANT Freeboard

Doc Ref: SICCI-ICESatANT-14-03

Version: 1.0

Date: 28 November 2014

Consortium Members

Change Record

Issue	Date	Reason for Change	Author
1.0D	30 June 2014	First draft, set-up of frame	Stefan Kern
2.0D	03 August 2014	Second draft	Stefan Kern
3.0D	07 November 2014	Final draft	Stefan Kern
1.0	28 November 2014	First Issue	Stefan Kern

Authorship

Role	Name	Signature
Written by:	Stefan Kern	
Checked by:	Gary Timms	
Approved by:		
Authorised by:		

Distribution

Organisation	Names	Contact Details
ESA	Pascal Lecomte	Pascal.Lecomte@esa.int
NERSC	Stein Sandven, Natalia Ivanova	Stein.Sandven@nersc.no; natalia.ivanova@nersc.no
CGI	Gary Timms	gary.timms@cgi.com;
Met.no	Thomas Lavergne, Lars Anders Breivik, Steinar Eastwood	t.lavergne@met.no; larsab@met.no; s.eastwood@met.no
DMI	Leif Toudal Pedersen, Rasmus Tonboe	ltp@dmi.dk; rtt@dmi.dk
DTU	Roberto Saldo, René Forsberg, Henriette Skourup	rs@space.dtu.dk; rf@space.dtu.dk; hsk@space.dtu.dk
FMI	Marko Mäkynen, Eero Rinne	marko.makynen@fmi.fi; eero.rinne@fmi.fi;
University of Hamburg	Stefan Kern	stefan.kern@zmaw.de;
University of Bremen	Georg Heygster	heygster@uni-bremen.de
University of Cambridge	Peter Wadhams, John Fletcher, Vera Djepa	pw11@cam.ac.uk; jfaf2@damtp.cam.ac.uk vd256@cam.ac.uk

Organisation	Names	Contact Details
MPI-M	Dirk Notz	dirk.notz@zmaw.de;
Ifremer	Fanny Ardhuin	Fanny.Ardhuin@ifremer.fr
AWI	Marcel Nicolaus, Stefan Hendricks	marcel.nicolaus@awi.de, stefan.hendricks@awi.de

Table of Contents

List of Figures

List of Tables

1 Introduction

1.1 Purpose and Scope

This document provides the results of Work Package WP 2300 of the ESA CCI Sea Ice ECV Project Option: Antarctic sea ice thickness distribution. The main goal of this work package was to retrieve total (sea ice + snow) freeboard for Antarctic sea ice from satellite laser altimeter data. More specifically, this document details the freeboard retrieval using data from the Geophysical Laser Altimeter System (GLAS) flown aboard the Ice Cloud and Land Elevation Satellite ICESat between 2003 and 2009.

1.2 Document Structure

Following the list of applicable documents and references, this document initially provides a short introduction to freeboard of Antarctic sea ice. Following this, Section 3 describes the different retrieval methods. Section 4 shows results of the retrieval method selected for WP2300 and details the uncertainty estimates. Section 5 gives the concluding recommendations.

1.3 Applicable Documents

The following table lists the Applicable Documents that have a direct impact on the contents of this document and should be read in conjunction with it.

Acronym	Title	Reference	Issue
AD-01	Sea Ice ECV Project Management Plan	ESA-CCI_SICCI_PMP_D6.1_v1.1	1.1
AD-02	ESA-CCI Scientific user consultation and detailed specification: Statement of Work (SoW)	EOP-SEP/SOW/0031-09/SP	1.4.2
AD-03	Annex E to the SoW	EOP-SEP/SOW/0031-09/SP	1.4.2

Table 1.3.1: Applicable Documents

1.4 Reference Documents

Acronym	Title	Reference	Issue
RD-01	SICCI_URD	SICCI-URD-03-12	1.3
RD-02	SICCI_ATBD	SICCI-ICESatANT-14-03	1.0
RD-03	ICESat's laser measurements of polar ice, atmosphere, ocean, and land	Zwally, H. J., et al., Journal of Geodynamics, 34, 405-445, 2002	n.a.

Acronym	Title	Reference	Issue
RD-04	Laboratory measurements of radar backscatter from bare and snow covered saline ice sheets	S. G. Beaven, G. L. Lockhart, S. P. Gogineni, A. R. Hosseinmostafa, K. Jezek, A. J. Gow, D. K. Perovich, A. K. Fung, and S. Tjuatja, International Journal of Remote Sensing, 16(5), 851-876	n.a.
RD-05	Evolution of first-year and second-year snow properties on sea ice in the Weddell Sea during spring-summer transition	Nicolaus, M., C. Haas, and S. Willmes, Journal of Geophysical Research, 114, D17109, doi:10.1029/2008JD011227, 2009	n.a.
RD-06	Snow on Antarctic sea ice	Massom, R. A., et al., Reviews in Geophysics, 39(3), 413-445, 2001	n.a.
RD-07	A description of the snow cover on the winter sea ice of the Amundsen and Ross Seas	Sturm, M., K. Morris, and R. A. Massom, Antarctic Journal of the US, 30(1-4), 21-24, 1995	n.a.
RD-08	Field investigations of Ku-Band radar penetration into snow cover on Antarctic sea ice	Willatt, R.C., K.A. Giles, S.W. Laxon, L. Stone-Drake and A.P. Worby, IEEE Transactions on Geoscience and Remote Sensing, 48(1), 365–372, 2010	n.a.
RD-09	High interannual variability of sea-ice thickness in the Arctic region	Laxon, S., N. Peacock, and D. Smith, Nature, 425, 947–950, 2003	n.a.
RD-10	CryoSat-2 estimates of Arctic sea ice thickness and volume	Laxon, S. W., et al., Geophysical Research Letters, 40, 1–6, 2013	n.a.
RD-11	ICESat over Arctic sea ice: Estimation of snow depth and ice thickness	Kwok, R. and Cunningham, G. F., Journal of Geophysical Research, 113, C08010, 2008	n.a.
RD-12	ICESat measurements of freeboard and estimates of sea-ice thickness in the Weddell Sea	Zwally, H. J., D. Yi, R. Kwok, and Y. Zhao, Journal of Geophysical Research, 113, C02S15, doi:10.1029/2007JC004284, 2008	n.a.
RD-13	ICESat observations of seasonal and interannual variations of sea-ice freeboard and estimated thickness in the Weddell Sea, Antarctica (2003–2009)	Yi, D., H. J. Zwally, and J. W. Robbins, Annals of Glaciology, 52(57), 43-51, 2011	n.a.
RD-14	Freeboard, snow depth and sea-ice roughness in East Antarctica from in situ and multiple satellite data	Markus, T., R. Massom, A. Worby, V. Lytle, N. Kurtz, and T. Maksym, Annals of Glaciology, 52(57), 242-248, 2011	n.a.
RD-15	Satellite observations of Antarctic sea ice thickness and volume	Kurtz, N. T., and T. Markus, Journal of Geophysical Research, 117, C08025, doi:10.1029/2012JC008141, 2012	n.a.

Acronym	Title	Reference	Issue
RD-16	Sea ice thickness estimations from ICESat Altimetry over the Bellingshausen and Amundsen Seas, 2003–2009	H. Xie, A. E. Tekeli, S. F. Ackley, D. Yi, and H. J. Zwally, Journal of Geophysical Research, 118, 2438-2453, doi:10.1002/jgrc.20179, 2013	n.a.
RD-17	Antarctic sea ice elevation from satellite radar altimetry	Giles, K., S. Laxon, and A. Worby, Geophysical Research Letters, 35, L03503, doi:10.1029/2007GL031572, 2008	n.a.
RD-18	Sea ice thickness retrieval algorithms based on in-situ surface elevation and thickness values for application to altimetry	Ozsoy-Cicek, B., S. F. Ackley, H. Xie, D. Yi, and J. Zwally, Journal of Geophysical Research - Oceans, 118, 3807-3822, doi:10.1002/jgrc.20252, 2013	n.a.
RD-19	An ultra-wideband, microwave radar for measuring snow thickness on sea ice and mapping near-surface internal layers in polar firn	Panzer, B., Gomez-Garcia, D., Leuschen, C., Paden, J., Rodriguez-Morales, F., Patel, A., Markus, T., Holt, B., and Gogineni, S. P., Journal of Glaciology, 59(214), 244-255, 2013	n.a.
RD-20	A method to automatically determine sea level for referencing snow freeboards and computing sea ice thicknesses from NASA IceBridge airborne LIDAR	X.Wang, H. Xie, Y. Ke, S. F. Ackley, and L. Liu, Remote Sensing of Environment, 131, 160-172, 2013	n.a.
RD-21	Ice, Cloud, and land Elevation Satellite (ICESat) over Arctic sea ice: Retrieval of freeboard	Kwok, R., G. F. Cunningham, H. J. Zwally, and D. Yi, Journal of Geophysical Research, 112, C12013, doi:10.1029/2006JC003978, 2007	n.a.
RD-22	Satellite-based estimates of sea ice volume flux through Fram Strait	Spreen, G., S. Kern, D. Stammer, R. Forsberg, and J. Haarpaintner, Annals of Glaciology, 44, 321–328, 2006	n.a.
RD-23	Uncertainties in Antarctic sea ice thickness retrieval from ICESat	Kern, S., and G. Spreen, Annals of Glaciology, 56(69), 107-119, doi:10.3189/2015AoG69A736, 2015	n.a.
RD-24	Sea ice freeboard in McMurdo Sound, Antarctica, derived by surface-validated ICESat laser altimeter data	Price, D., W. Rack, C. Haas, P. J. Langhorne, and O. Marsh, Journal of Geophysical Research, 118, 3634-3650, doi:10.1002/jgrc.20266, 2013	n.a.
RD-25	ICESat swath and gridded freeboard and ice thickness for Antarctic	NASA Cryosphere Science Research Portal at National Aeronautics and Space Administration (NASA), 2013, http://seaice.gsfc.nasa.gov/csb/index.php?section=272	1.0

Acronym	Title	Reference	Issue
RD-26	GLAS/ICESat L2 Sea Ice Altimetry Data	Zwally, H., R. Schutz, C. Bentley, J. Bufton, T. Herring, J. Minster, J. Spinhirne, and T. Ross (2011). Version 33. [Periods 2B to 3G]. Boulder, Colorado USA: National Snow and Ice Data Center	n.a.
RD-27	ICESat data	National Snow and Ice Data Center, NSIDC, 2013a, http://nsidc.org/data/gla13.html	n.a.
RD-28	Software to read ICESat data	National Snow and Ice Data Center, NSIDC, 2013b, http://nsidc.org/data/icesat/tools.html	n.a.
RD-29	The development and evaluation of the Earth Gravitational Model 2008 (EGM2008)	Pavlis, N. K., S. A. Holmes, S. C. Kenyon and J. K. Factor, Journal of Geophysical Research, 117, B04406, doi:10.1029/2011JB008916, 2012	n.a.
RD-30	A range correction for ICESat and its potential impact on ice-sheet mass balance studies	Borsa, A. A., G. Moholt, H. A. Fricker, and K. M. Brunt, The Cryosphere, 8, 345-357, 2014	n.a.
RD-31	Sea ice remote sensing using AMSR-E 89 GHz channels	Spreen, G., L. Kaleschke, and G. Heygster, Journal of Geophysical Research, 113, C02S03 doi:10.1029/2005JC003384, 2008	n.a.
RD-32	SSM/I Sea Ice Remote Sensing for Mesoscale Ocean-Atmosphere Interaction Analysis	Kaleschke, L., C. Lüpkes, T. Vihma, J. Haarpaintner, A. Bochert, J. Hartmann, and G. Heygster, Canadian Journal of Remote Sensing, 27(5), 526-537, 2001	n.a.
RD-33	Thinning and Volume Loss of the Arctic Ocean Sea Ice Cover: 2003–2008	Kwok, R., G. F. Cunningham, M. Wensnahan, I. Rigor, H. J. Zwally, and D. Yi, Journal of Geophysical Research, 114, (C07005), doi:10.1029/2009JC005312, 2009	n.a.
RD-34	Validating ICESat over thick sea ice in the Northern Canada Basin	Connor, L. N., S. L. Farrell, D. McAdoo, W. B. Krabill, and S. Manizade, IEEE Transactions on Geoscience and Remote Sensing, 51(4), 2188-2200	n.a.
RD-35	ICESat observations of Arctic sea ice: A first look	Kwok, R., H. J. Zwally, and D. Yi, Geophysical Research Letters, 31, L16401, doi:10.1029/2004GL020309, 2004	n.a.
RD-36	An algorithm to detect sea ice leads by using AMSR-E passive microwave imagery	Röhrs, J., L. Kaleschke, D. Bröhan, and P. K. Siligam, The Cryosphere, 6, 343-352, 2012	n.a.

Table 1.4.1: Reference Documents

1.5 Acronyms and Abbreviations

Acronym	Meaning
ACDD	Attribute Convention for Dataset Discovery
ATBD	Algorithm Theoretical Basis Document
CCI	Climate Change Initiative
CF	Climate and Forecasting
DMSP	Defence Meteorological Satellite Program
EASE	Equal Area Scalable Earth-Grid
ECV	Essential Climate Variable
Envisat	Environmental Satellite
EO	Earth Observation
ERS	European Remote Sensing Satellite
FB	Freeboard
GCOS	Global Climate Observing system
GHRSST	Group for High Resolution Sea Surface Temperature
GLAS	Geophysical Laser Altimeter System
ICESat	Ice, Cloud and land Elevation Satellite
IDL	Interactive Data Language
Matlab	Matrix Laboratory
MIZ	Marginal ice zone
n.a.	Not applicable
netCDF	Network Common Data Format
NH	Northern hemisphere
NSIDC	National Snow and Ice Data Centre
OIB	Operation Ice Bridge
OSI-SAF	Ocean and Sea Ice Satellite Application Facility
PDGS	Payload Data Ground System
RA	Radar altimeter
SH	Southern hemisphere
SIC	Sea Ice Concentration
SICCI	Sea Ice Climate Change Initiative
SIT	Sea Ice Thickness
SMMR	Scanning Multichannel Microwave Radiometer
SMOS	Soil Moisture and Ocean Salinity
SSM/I	Special Sensor Microwave / Imager
TBD	To be defined
URD	User Requirements Document

Table 1.5.1: Acronyms

2 Introduction to Freeboard of Antarctic Sea Ice

Sea ice floats on sea water. A small part of the sea ice projects out of the water while the majority of it remains in the water. The latter is the so-called draft while the former is the so-called freeboard. Draft and freeboard are both functions of the sea ice density, the sea water density and the density and thickness of a snow cover on top of the sea ice. Freeboard might also be a function of the mobility and degree of deformation of the sea ice. The buoyancy of a freely floating sea ice floe is determined by its density and thickness but could be disturbed in case the sea ice floe is within a matrix of other floes exerting some bending or other forces.

The part of the sea ice projecting out of the water is called sea ice freeboard independent of a snow cover. If one considers both, the sea ice and its snow cover then one speaks of the total (sea ice + snow) freeboard. Total and sea ice freeboard are the same in case of bare sea ice.

This report focusses on measurements of the Geophysical Laser Altimeter System (GLAS) aboard the Ice Cloud and Elevation Satellite ICESat-1 [RD-03]. The GLAS instrument is a laser altimeter operating at wavelengths of 532 nm and 1064 nm. The penetration depth into the sea ice and its snow cover is therefore of the order of millimetres and hence ICESat GLAS observations can be converted into a measure of the total freeboard, as described in Section 3. The laser altimeter sees the snow surface.

For Antarctic sea ice, using laser altimetry could be an advantage over using radar altimetry. Radar altimeters are typically operating at frequencies in Ku-Band, that is 12 GHz – 18 GHz. At this frequency band, laboratory studies have shown that the main reflecting horizon is the ice-snow interface [e.g. RD-04] and hence it can be assumed that radar altimetry can be used to infer the sea ice freeboard. However, Antarctic sea ice is not quite similar to the conditions encountered in those laboratory studies. The frequent change in surface air temperature combined with changing wind directions and frequent precipitation events in many places on Antarctic sea ice causes a vertically heterogeneous snow cover [e.g. RD-05; RD-06; RD-07]. The Antarctic snow cover can have several buried icy layers. In addition flooding of the ice-snow interface and/or percolation of meltwater from the top of the snow cover can cause formation of snow ice or meteoric ice at the ice-snow interface. Consequently, at the ice-snow interface, density and salinity gradients and hence also gradients in di-electric properties relevant for radar signal reflection and/or backscatter become less distinct. Because of this the ice-snow interface is not as clearly defined anymore [e.g. RD-08]. The spatiotemporal distribution of these effects is however not yet known and it can still be assumed that for the bulk of the Antarctic sea ice the assumption of Beaven et al. [RD-04] holds.

We note that the above-mentioned environmental conditions and processes also impact the quality of snow depth retrieval on sea ice using satellite passive microwave data. This will be detailed in the deliverables D1.1 and D1.2 of the SICCI-Project ANT SIT Option.

Both, sea ice and total freeboard are used to compute sea ice thickness. For the Arctic, conversion of freeboard into thickness is relatively mature and is described in a variety of publications, e.g. Laxon et al. [RD-09, RD-10] for radar altimetry and e.g. Kwok and Cunningham [RD-11] for ICESat. For the Antarctic, however, methods are less mature and provide different results for sea ice thickness when based on ICESat [RD-12; RD-13; RD-14; RD-15; RD-16] or point to limitations when using radar altimetry [RD-17]. Pre-requisite for all approaches to compute sea ice thickness cited above is the freeboard, however.

We note that total freeboard measurements exist in the form of in situ drillings from various field expeditions into the Southern Ocean. The bulk of these measurements have been compiled and analysed in Ozsoy-Cicek et al. [RD-18]. Such measurements are however very local and are spread largely over time and regions and therefore do not provide sufficient information about the Antarctic freeboard distribution.

The second source of total freeboard measurements are data obtained during the flights of the Operation Ice Bridge (OIB) campaigns. These started in 2009 to fill the data gap between ICESat-1 and ICESat-2 to be launched in 2017. Instruments used aboard the OIB flights are described in Panzer et al. [RD-19]. OIB data have been used by various groups in the Arctic but have not yet found too many users in the Antarctic [Wang et al., RD-20].

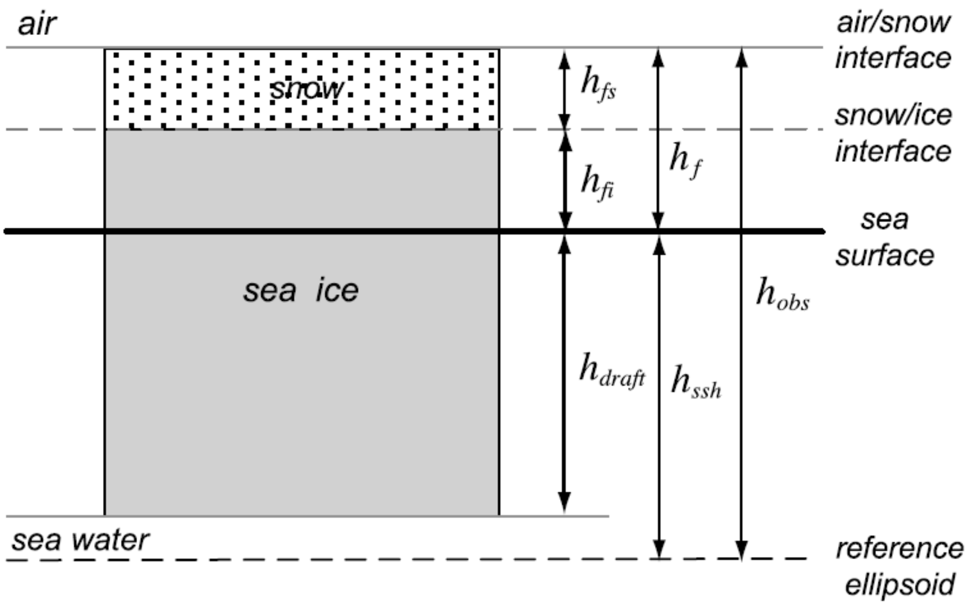

Figure 1.5.1 Illustration of the quantities involved in laser altimetry of sea ice. h_f is total freeboard, h_{fs} is snow depth, and h_{fi} is the elevation of the snow/ice interface over the sea surface, also called sea ice freeboard. Figure taken from RD-21.

3 Methods to retrieve total freeboard for Antarctic sea ice

This section provides brief descriptions of methods used to infer total freeboard from ICESat GLAS measurements.

3.1 ICESat-1

The ICESat-1 satellite was launched in 2003 with multiple goals [RD-03]. The ICESat-1 GLAS instrument allowed to measure elevations for up to three periods of up to 35 days duration each year during its lifetime. ICESat-1 measurement periods were usually in February/March, May/June, and October/November during years 2003 to 2009 [e.g. RD-13]. Due to various reasons the most useful measurement periods are those from 2004 to 2008; for 2004-2006 there are three measurement campaigns per year; in 2007 and 2008 measurements were limited to February/March (in 2007: March/April) and October/November.

The laser of the GLAS instrument allows to obtaining the distance between the sensor and the surface with a few centimetre accuracy via runtime measurement of the laser pulse between the sensor and the surface. The footprint illuminated at the surface by one laser shot is almost circular and approximately 60 m in diameter. The footprint centres of consecutive laser shots are separated by about 172 m. More details about the ICESat-1 satellite, the GLAS sensor, and the data released can be found in Zwally et al. [RD-03] and on the ICESat webpage.

The single laser shot elevation accuracy is given as 13.8 cm [RD-03].

3.2 The concept

Figure 3.1 illustrates the concept to derive total freeboard from GLAS elevation measurements. The satellite knows its position relative to the reference ellipsoid of the Earth: h_{ellip}. The sensor measures the distance to whatever surface is reflecting the laser pulse at the Earth: D_{laser}. The freeboard F can then be computed with the following equation [RD-21; RD-22]:

$$F = h_{ellip} - D_{laser} - h_{geoid} - h_{tides} - h_{atm} - h_{dyn}$$

Here h_{geoid} is the height of the Earth geoid above the ellipsoid. The h_{tides} includes the influence of the ocean and Earth tides on the measured elevation and h_{atm} is the impact of the atmospheric loading on the sea surface. Finally h_{dyn} describes the impact by the ocean itself on the sea surface height (SSH) like currents and other second-order terms like steric SSH changes. All these contributions except h_{dyn} are known and/or approximated using models in a reasonable way and are taken into account in the ICESat-1 GLAS laser altimeter product used: GLA13. Only h_{dyn} is unknown. Knowledge of h_{dyn} with centimetre accuracy is a prerequisite for retrieval of F. Currently, h_{dyn} is not known with the required spatiotemporal resolution and therefore this part of the SSH needs to be approximated in a different way. The methods described below therefore exactly target the SSH approximation from other sources and/or ICESat-1 data itself.

Methods developed to obtain freeboard using ICESat-1 data in the Arctic [e.g. RD-21; RD-22] were modified for the Antarctic by, e.g., Zwally et al. [RD-12]. As stated above, the main difficulty is to approximate the local SSH. Only with the knowledge of the SSH ICESat-1 elevation measurements can be converted into freeboard. One way to find SSH within the ice cover is to combine ICESat-1 elevation measurements with contemporary high-resolution optical or synthetic aperture radar imagery. Where the latter indicates fresh leads, i.e. open water or thin ice areas in the sea ice cover, a collocated ICESat-1 elevation measurement can be assumed to represent the local SSH. This method has two severe caveats. At first, one needs collocated imagery of the mentioned kind for each ICESat-1 overpass. In case of using optical data these even need to be cloud free and obtained under daylight conditions. Secondly, one needs such data at a spatial resolution which is comparable to the footprint size of the GLAS instrument: about 60 m. Neither MODIS imagery nor Envisat ASAR imagery or similar satellite imagery can be reliably used for this purpose therefore; their spatial resolutions are 250 m and 150 m (WideSwathMode for Envisat ASAR to have sufficient spatial coverage). This method was discussed in Kwok et al. [RD-21] and has not been used further for ICESat-1 freeboard retrieval in the Arctic. Instead the concept is to find leads or, in other words, minima of the measured elevation, in the ICESat-1 data themselves. This can be done, e.g., using the so-called lowest level elevation method described in the following section. It was first published for the Antarctic by Zwally et al. [RD-12] and has been applied and investigated by Yi et al. [RD-13], Xie et al. [RD-16] and Kern and Spreen [RD-23].

3.3 Lowest Level Elevation method

The basic idea of the lowest level elevation method is to find elevations which can be taken as SSH tie points which can subsequently be used to approximate the SSH along the considered ICESat-1 ground track. Once the SSH is known it can be subtracted from the elevation residua obtained from the ICESat-1 measurements. These elevation residua result from evaluating the equation given above except h_{dyn} which is unknown but approximated by the SSH derived with the lowest level elevation method. Before minima are identified the elevations of each track are filtered with a high-pass filter to remove large-scale variations. To find SSH tie points a search window is moved along the ground track over the elevation residua. Elevation minima are sought within that window. This is done by sorting all valid elevations within that window and selecting a percentage P of the lowest values as the sought minimum elevations. Yi et al. [RD-13] and Zwally et al. [RD-12] used 2% for P for the Weddell Sea. In a more regional study of McMurdo Sound Price et al. [RD-24] suggested to use 5%. The search window can either be moved in fixed increments of, e.g., half the window width or the search window can be centred at each laser shot location and moved by one shot [RD-13].

The number of leads (or minima) found is a function of the length of the search window (Figure 3.3.1). If the search window is too short then it might not cover any lead. Since the method still picks the minimum elevations it is likely that these are not associated with leads. Consequently the SSH tie points are positively biased as is the SSH obtained from these. A positively biased SSH however yields a negatively biased freeboard and thus sea ice thickness. If the search window is very long then one can be sure that enough leads are hit. However a too long search window of, say 100 km length, cannot take into account SSH variations on the scale of a few ten kilometres as is illustrated in Fig. 3.3.2. If there is a gradient in the SSH within the search window with rather low values at one end and rather high values at the other end of the search window, the minima identified by the method are representing the SSH close to the end with the low SSH values. Consequently, the SSH distribution within the search window is not approximated correctly. More specifically, the SSH is going to be negatively biased in the part of the search window exhibiting the rather high SSH values, which will cause a positive bias in freeboard and consequently ice thickness.

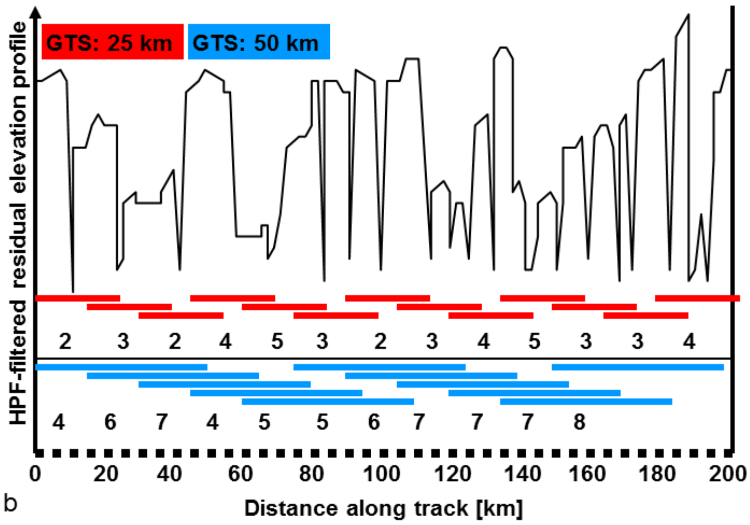

Figure 3.3.1 Illustration of the effect on the number of identified minima for two different search window lengths (Ground Track Segment GTS) for an artificial residual elevation profile. Red and blue bars denote the length and location of the GTS which are shifted by 15 km. Figures below these bars denote the number of leads found (taken from [RD-23]).

Input parameters to the lowest level elevation method therefore need to be a trade between:

- resolving local SSH variations as accurate as possible and hence using an as short as possible GTS

and

- finding enough minima which are actually really leads and hence using an as large as possible value for the percentage P defining which of the elevations are taking as SSH tie points.

However, the choice of P should be determined by the actual fraction of leads in the sea ice cover. If for example there are less than 5 leads / 100 km GTS then P needs to be smaller than 5%. Otherwise elevation minima which are not associated with leads are taken as SSH tie points. A choice of P = 3 or 2 would be fine. We note that it also needs to be taken into account that even if there are enough leads present these need to be hit by the laser which only provides one shot every 172 m.

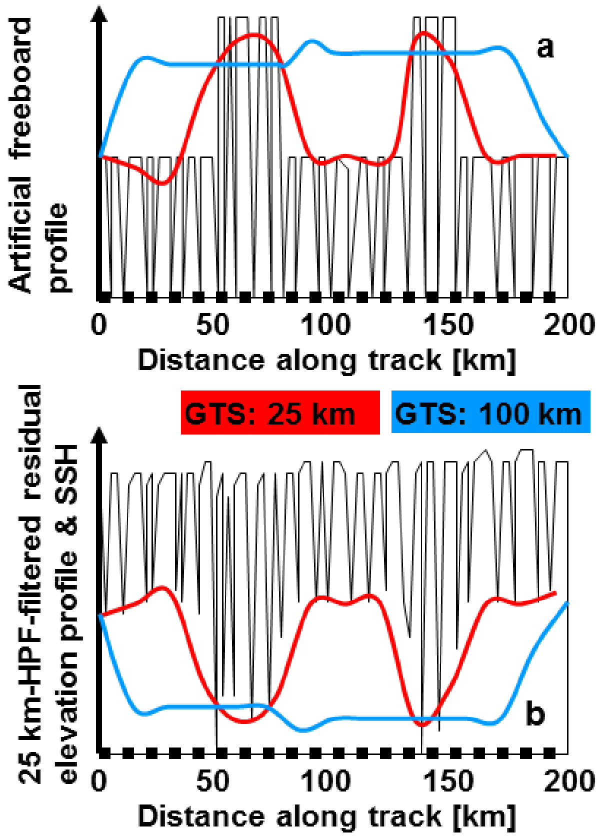

Figure 3.3.2 Illustration of the effect of two different GTS lengths (25km and 100km) on the approximation of the SSH (b) and retrieval of the freeboard (a). With a GTS of 100 km the details which are maintained in the elevation residua by the high-pass filtering are not resolved (taken from [RD-23]).

3.4 Modified Lowest Level Elevation method

Markus et al. [RD-14] modified the lowest level elevation method [RD-12; RD-13] by including lessons learned from work done in the Arctic by Kwok et al. [RD-21]. Markus et al. [RD-14] used optical imagery of two ICESat-1 measurement periods (Oct./Nov. 2003 and May/June 2005) to obtain a relationship between the elevation standard deviation over the scale of 25 km and elevation minima within the same 25 km ground track. The empirical relationship is subsequently used to derive a possible range of SSH tie points as a function of the elevation standard deviation. For a given elevation standard deviation the minima selected from the elevation residua are required to be within ±7 cm of the elevation corresponding to the respective elevation standard deviation (see [RD-14], figure 5). The selection of the minima is the same as in our case instead that the GTS used in Markus et al. [RD-14] is 25 km instead of 50 km and that instead of using a percentage P always the 3 lowest elevation residua are taken as minima. If the minima do not fulfil the above-mentioned criterion then no freeboard is retrieved for this particular laser shot. More details of this approach can be found in Markus et al. [RD-14] and Kurtz and Markus [RD-15].

The data obtained with this method are available from NASA as single laser shot as well as gridded (25 km) product via: Cryosphere Science Research Portal at National Aeronautics and Space Administration [RD-25] and are used in this study for inter-comparison.

3.5 Approach for the SICCI project

The results are based on GLAS/ICESat L2 Sea Ice Altimetry Data (GLA13) of the release 33 [RD-26]. The data is downloaded for ICESat-1 measurement periods 2B to 3G (February/March 2004 to October/November 2006) from NSIDC [RD-27]. The data is pre-processed with software provided by the National Snow and Ice Data Centre [RD-28]; here the Interactive Data Language (IDL) readers are used. As is recommended in Zwally et al. [RD-26] the following corrections and flags are applied to the surface elevations: i_reflctUC, i_reflCor_atm, i_gval_rcv, i_Surface_pres, i_satElevCorr, i_satCorrFlg. Resulting surface elevations are given relative to the EGM08 geoid [RD-29] provided together with the ICESat data (i_gdHt). We did not carry out the G-C offset correction [RD-30].
Elevations higher than 4 m above the geoid are removed to discard icebergs [RD-12]. Secondly, residual elevation profiles are computed by subtracting an along-track averaged elevation profile from the original elevation profile. The result is a high-pass filtered residual elevation containing only small spatial-scale variations in surface elevation of up to several ten centimetres. The width of the window used for averaging is referred to as high-pass filter (HPF) width henceforth.
For the approximation of SSH from surface elevation residuals we use the lowest-level elevation method (see section 3.3). A window of length X, called ground track segment (GTS) henceforth, is moved along the elevation profile. Within the segment elevations are sorted in ascending order and the lowest percentage (P) elevations are identified. These elevation minima are assumed to be caused by new leads with open water or very thin ice and are used as tie points to approximate SSH which is subsequently subtracted from the elevations to obtain total freeboard.
The parameters HPF, GTS, P are crucial for the freeboard retrieval using the lowest level elevation method. Kern and Spreen [RD-23] carried out a sensitivity study of this method to these parameters. It is yet difficult to carry out a sophisticated validation study of ICESat-1 freeboard obtained in the Southern Ocean simply because of the lack of coincident independent freeboard observations. Therefore such a sensitivity study can be regarded as a reasonable alternative. The main results of Kern and Spreen [RD-23] are that i) GTS must not be larger than HPF, ii) the choice of P is crucial and should be chosen in accordance with the lead concentration obtained from an independent product but a value of 2% seems to be a valid compromise, iii) a trade-off has to be found between an as fine as possible spatial resolution and the minimum number of leads to be identified within a GTS to

allow reliable SSH approximation. The setting chosen for the SICCI project is hence: P=2%, GTS length: 50 km, HPF length: 50 km.
Freeboard is computed only for ice covered areas. We used sea ice concentrations calculated with the Artist Sea Ice (ASI) concentration algorithm [RD-31; RD-32] applied to 85 GHz Special Sensor Microwave/Imager (SSM/I) observations. ASI sea ice concentrations are taken from the Integrated Climate Data Center [ICDC, 2013] as 5-day median filtered gridded product with daily temporal and 12.5 km grid resolution. For higher sea ice concentration in the range used here, uncertainty estimates are of the order of 5 % [RD-31]. Only grid cells with a sea ice concentration above 60% are used unless stated otherwise.
Freeboard is calculated for single laser shots, i.e. stored as latitude, longitude, freeboard estimate. Freeboard and mean single shot laser uncertainty is also computed in form of gridded tracks, i.e. for every day all ICESat-1 overpasses are taken, freeboard is computed along the overpasses and subsequently gridded into the NSIDC polar-stereographic grid with tangential plane at 70°S. Grid resolutions used are 25 km (according to Yi et al., [RD-13]) and 100 km to comply with the radar altimeter product and to allow a more complete coverage of the Southern Ocean with gridded freeboard data. All gridded daily freeboard (and uncertainty) data are then composited into an average freeboard (and uncertainty) map for every ICESat-1 measurement period.

3.6 Uncertainty estimation

For the Arctic contemporary airborne observations of the total freeboard allowed direct validation of total freeboard obtained from ICESat-1 [e.g. RD-33; RD-34]. ICESat-1 elevation measurement precision is of the order of 0.02 m [RD-35] and the elevation accuracy is about 0.03 to 0.04 m [RD-34].

For the Antarctic, such measurements do not exist. We could, in principle, simply take a constant uncertainty value by combining the above-mentioned two numbers: 0.02 m and 0.03 to 0.04 m, adding up to an uncertainty value of about 0.03 m. But this would not reflect the large spatial variability of valid ICESat-1 measurements per grid cell. Also the results of Connor et al. [RD-34] might not be valid for the Weddell Sea or Antarctica in general.

From our computations (see Section 4) we see that the single laser shot precision of 0.138 m translates into a per-grid cell contribution to the total freeboard uncertainty of about 0.01 to 0.02 m which varies with the number of valid ICESat-1 measurements. The sensitivity study [RD-23] revealed: total freeboard as obtained with the lowest level elevation method can change as a function of input parameters to this method, by between 0.05 and 0.10 m over large areas. Therefore, to have a more reasonable estimate of total freeboard uncertainty to be used for the error propagation within the SICCI project for the freeboard-to-thickness conversion than the standard deviation of the mean freeboard suggested in Yi et al. [RD-13], and to comply with the above-mentioned studies we apply an empirical factor of 3 to the calculated mean single laser short precision and use the result as freeboard error estimate σ_F. This results in a gridded total freeboard uncertainty which is at least 0.03 m for the entire region of interest and which distribution takes into account the number of valid measurements per grid cell. The choice of a value of 3 for this empirical factor is still kind of arbitrary and the factor might need to be even higher. However, without further evaluation data to quantify the difference between measured and actual surface elevation there is limited added value in further refining such an empirical factor. It is meant to allow a per-grid cell estimate of total freeboard uncertainty which takes the varying number of valid ICESat-1 elevation measurements into account and which allows us to finally give a per-grid cell estimate of sea ice thickness uncertainty.

4 Antarctic Sea Ice Total freeboard from ICESat-1: Results and Uncertainties

This section contains the results of the (modified) Yi et al. [RD-13] approach plus the uncertainties as is described in the previous section; see also Kern and Spreen [RD-23]. We first show a few results from the lowest-level elevation method (LLEM) sensitivity study [RD-23]. Subsequently we report on retrieved freeboards and uncertainties before we compare our freeboard with the freeboard obtained from NASA [RD-14; RD-15] and give an outlook towards improved quantification of the freeboard uncertainty.

4.1 Freeboard along single tracks: Sensitivity to LLEM input parameters

The width of the high-pass filter (HPF) to remove large-scale SSH variations from the observed elevations, the length of the ground track segment (GTS) used to search elevation minima, and the percentage (P) used to define which elevation minima are taken as SSH tie points are input parameters for the LLEM. The sensitivity to these parameters is investigated by applying different combinations of these parameters and compared to the results with those of a "master setting": P = 2%, HPF = 50 km, GTS = 50 km.

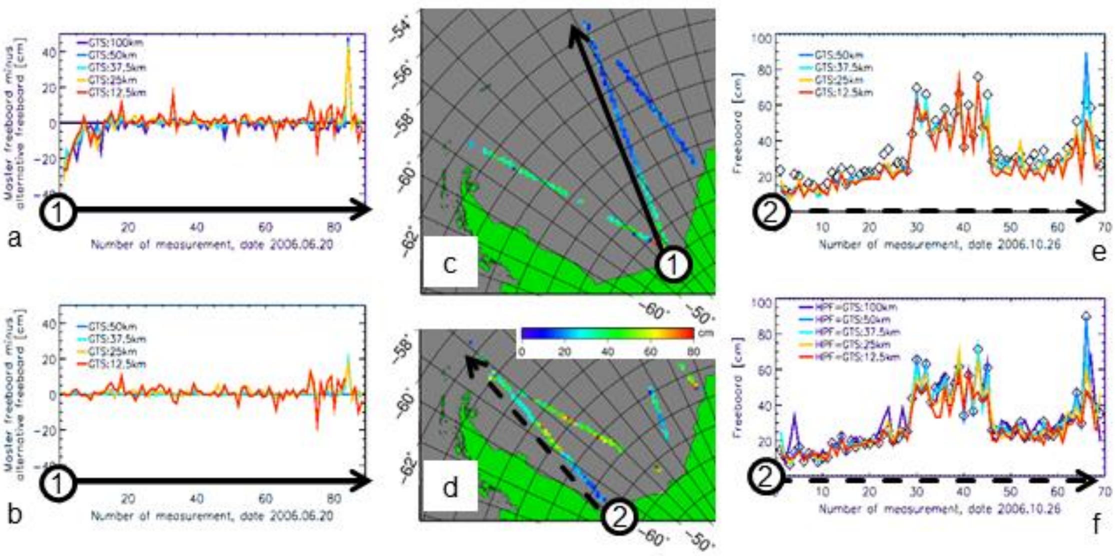

Figure 4.1.1 Illustration of freeboard retrieval parameter choice impact on two selected ICESat-1 tracks delineated in images c) and d). Image a) freeboard difference of master minus alternative setting (see text for details) for different ground track segment (GTS) lengths using no high-pass filter (HPF). Image b) freeboard difference master minus alternative setting for different GTS lengths for HPF=50km. Image e) freeboard for different GTS length, HPF=50km, for lowest level elevation method percentage P=5% (lines) compared to master setting (uses P=2%, diamonds). Image f) freeboard for different HPF=GTS combinations (lines) in comparison to the master setting (diamonds) (taken from [RD-23]).

Figure 4.1.1 a) reveals for the profile chosen, independent of GTS length, total freeboard is under-estimated relative to the master setting over about the first 10 grid cells - which corresponds to a distance of about at least 250 km – if no high-pass filter is applied (HPF=0%).
For Figure 4.1.1 b) for the same profile GTS length is varied while all other parameters are kept constant. Absolute differences remain local and below 0.10 m for the majority of the profile independent of GTS length.
Using a larger percentage P is supposed to cause a decrease in obtained total freeboard as long as enough leads are present; otherwise total freeboard is likely to be over-estimated in comparison to using a lower percentage P. Figure 4.1.1 e) gives an example of the first case: freeboard derived for the profile shown in Figure 4.1,1 d) with P=5% (colored lines) is smaller than freeboard derived for this profile with the master setting P=2% (diamonds); the difference is between 0.05 and 0.10 m. This seems to be more or less independent of GTS length.
Finally in Figure 4.1.1 f) we demonstrate for the profile shown in Figure 4.1.1 d) whether a change in HPF and GTS, here setting HPF=GTS, changes freeboard in comparison to the master setting. Total freeboard obtained for HPF=GTS=12.5 km (red line) tends to give the lowest values while total freeboard obtained for HPF=GTS=100 km (dark blue line) tends to give the largest values. Usage of a longer segment potentially causes a freeboard over-estimation compared to usage of a shorter segment; this is in line with the discussion in section 3.3.

4.2 Weddell Sea freeboard maps: Sensitivity to input parameters

Figure 4.2.1 a) elaborates on Figure 4.1.1 a) and shows an area of negative freeboard differences stretching along the Antarctic coast. Differences exceed 0.10 m, illustrating that omission of the high-pass filtering can lead to a notable over-estimation of total freeboard compared to the master setting. Most of the remaining area reveals differences close to zero. Along the ice edge differences tend to be larger as well, however both positive and negative differences are observed here. The histogram in Figure 4.2.1 b) shows an asymmetric distribution with mode and median being only slightly negative: -0.005 m and -0.021 m, respectively. If considering all nine ICESat-1 measurement periods in 2004-2006 then omission of the high-pass filtering cause higher freeboard values along the coast but has a rather small influence on the overall modal and mean total freeboard.
Figure 4.2.1 c) elaborates on Figure 4.1.1 e) and shows that using P=5% instead of P=2% causes wide-spread overestimation of total freeboard compared to the master setting. The histogram (Figure 4.2.1 d) is also asymmetric and exhibits a clear positive mode at 0.025 m and a mean of 0.036 m. Positive differences dominate and exceed 0.10 m. The mean difference to the master setting for the nine ICESat-1 measurement periods in 2004-2006 takes a value 0.06 m for modal total freeboard and between 0.04 and 0.06 m for mean total freeboard.
Using GTS = 25 km instead of GTS = 100 km causes both positive and negative differences in total freeboard; absolute values can exceed 0.10 m. Regional patterns are difficult to identify (Figure 4.2.1 e). Large negative differences, for example GTS = 100 km provides larger freeboard than GTS = 25 km, seem to be more present in the central Weddell Sea while large positive differences occur in some areas along the coast and along the ice edge. The overall mean difference is zero (Figure 4.2.1 f).

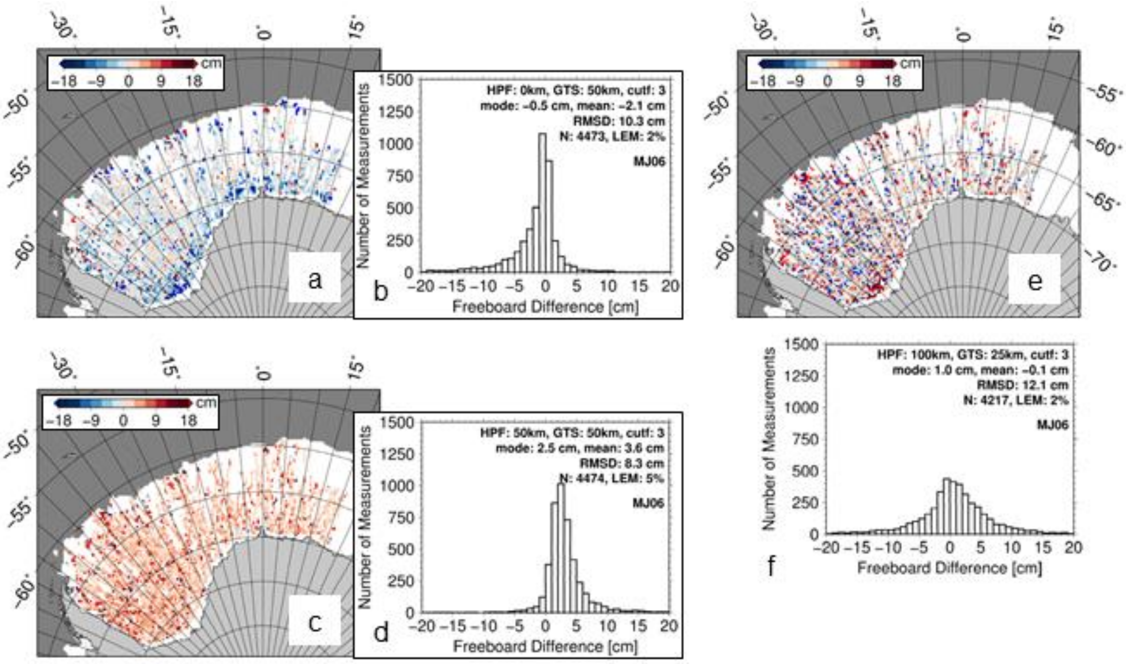

Figure 4.2.1 Difference of total freeboard obtained for ICESat-1 measurement period 3F (May/June 2006) with the master minus the alternative setting using a) no high-pass filter, and c) a percentage P=5%. Images b) and d) show histograms associated with a) and c). Image e) shows the difference in total freeboard using HPF = 100 km, GTS = 25 km minus freeboard using HPF = GTS = 100 km together with the corresponding histogram. White areas display the ICESat-1 measurement period mean sea ice extent using a 30% sea ice concentration threshold. Grid size is 25 km (taken from [RD-23]).

4.3 Freeboard obtained with the SICCI approach

Weddell Sea

Figure 4.3.1 gives an overview about the freeboard distribution in the Weddell Sea for ICESat-1 measurement periods from Februars/March 2004 (FM04) to February/March 2008 (FM08). Distribution and mean freeboard values agree well with the results of Yi et al. [RD-13]; the mean Weddell Sea freeboard for 2004-2006 agrees within 0.01 m with the results of Yi et al. [RD-13]. The maps shown in Figure 4.3.1 reveal white areas of different extent. These are areas without valid ICESat-1 freeboard measurements but a sea ice concentration above the chosen threshold of 60%. Here, ICESat-1 data are discarded because of forward scattering issues, too low gain, and other processing related inconsistencies. In contrast to Zwally et al. [RD-12] and Yi et al. [RD-13] we did not interpolate between the ICESat-1 tracks.

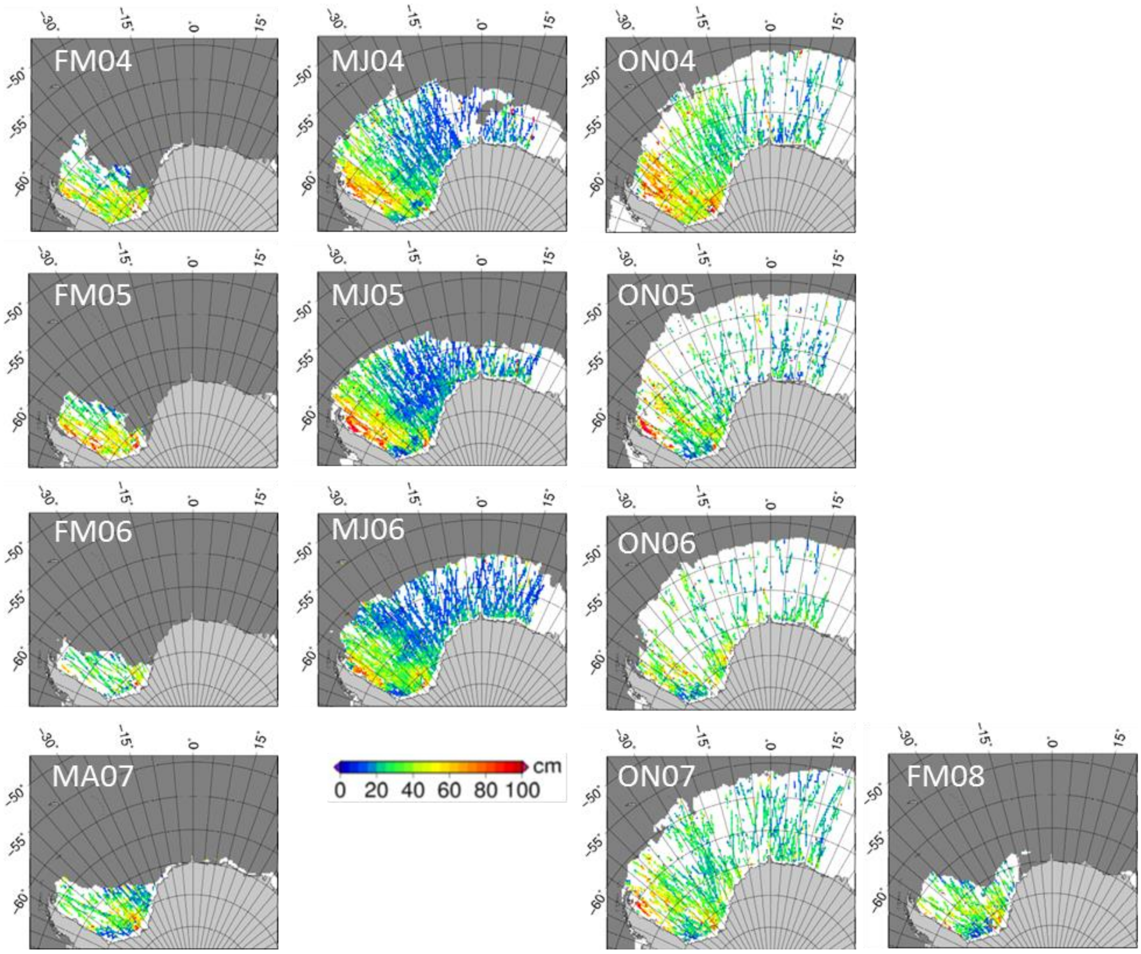

Figure 4.3.1 Freeboard distribution (SICCI approach) for February/March 2004 (FM04) to February/March 2008 (FM08) for the Weddell Sea. White areas denote regions with sea ice concentration above 60% but no valid ICESat freeboard data. Grid size is 25 km.

The freeboard distributions for fall (February/March) reveal an area of mostly high freeboards in the southern and south-western Weddell Sea in agreement with the expected location of perennial sea ice. A relatively small area of smaller freeboard indicates the started new ice formation. The freeboard distributions for early/midwinter (May/June) reveal large freeboard hugging the Antarctic Peninsula and extending into the north-western and northern Weddell Sea. Larger freeboards are also evident in the south-eastern Weddell Sea and towards the coasts. In the central and eastern Weddell Sea lower freeboard values dominate. The freeboard distributions for late winter / spring (October/November) show a similar pattern as those for May/June but with extended areas of larger freeboards along the coasts as well as a general increase in freeboard compared to May/June. We note that details in the ice cover such as the thinner sea ice downwind of the Ronne-Filchner Shelf Ice polynya in the Southern Weddell Sea as well as polynyas in the lee of the fast ice cover in the south-eastern Weddell Sea and the Larsen Ice Shelf polynya area can be identified.

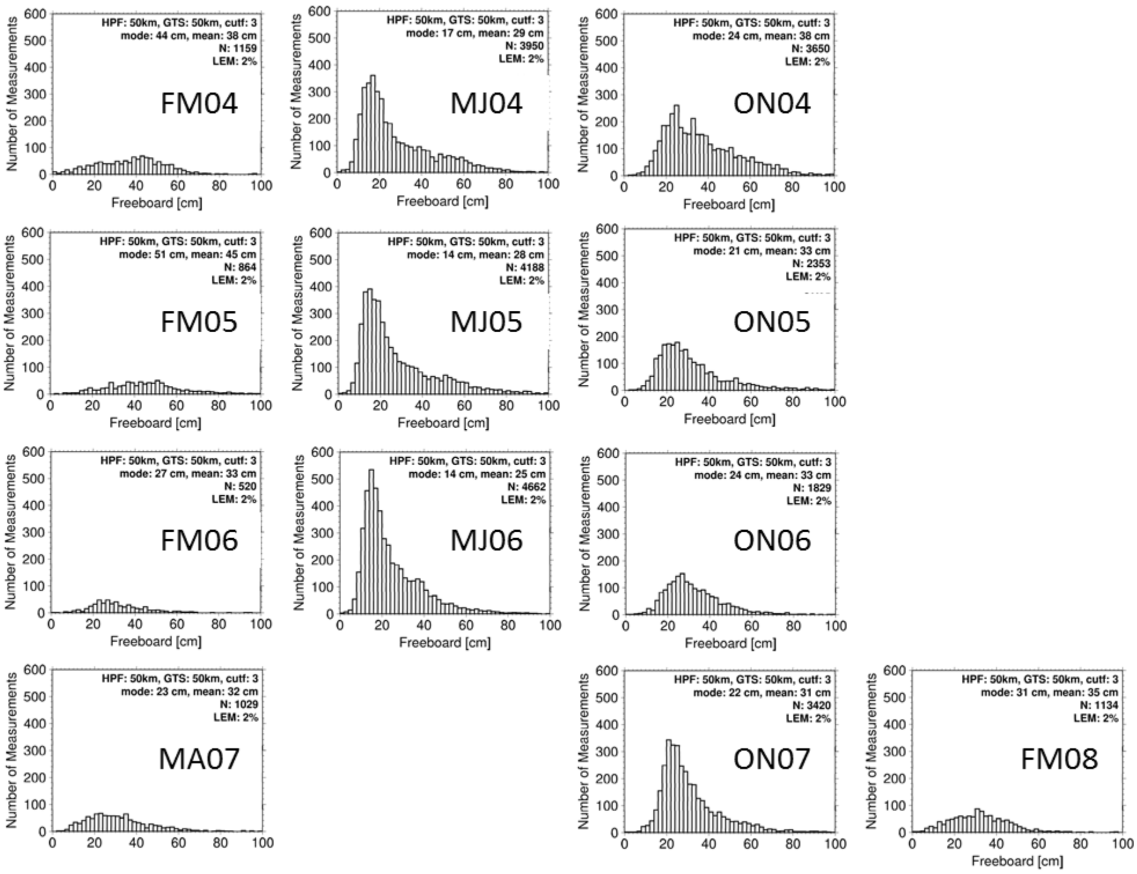

Figure 4.3.2 Histograms to the freeboard distribution shown in Figure 4.3.1.

The histograms corresponding to the maps shown in Figure 4.3.1 are given in Figure 4.3.2 and underline what has been just discussed. We note that histograms of May/June and October/November reveal modal values of the freeboard which increase as the season progresses.

Kwok et al. [RD-21] suggested to using the reflectivity measured by ICESat-1 to distinguish between fresh leads and thick and/or snow covered sea ice. This seems to work fine in the Arctic. In a preliminary study (results are not shown here) Envisat ASAR images were collocated with ICESat-1 elevations and reflectivity in order to assess whether the results of Kwok et al. [RD-21] are also valid in the Antarctic. The profiles should compare in a way that leads identified in the ASAR images should coincide with elevation minima and reflectivity minima. The latter was not the case, however; in about 50% of the cases investigated the reflectivity did not drop below 0.5, a value suggested by Kwok et al. [RD-21] to be a reliable indicator of leads. If we apply such a filter in the Antarctic and allow only those elevation minima to be used as SSH tie points which exhibit a reflectivity below 0.5 then we end up with a much sparse data coverage, more outliers and a higher mean freeboard for the Weddell Sea (compare left image, SICCI approach, with right image, SICCI approach with reflectivity filter in Figure 4.3.3).

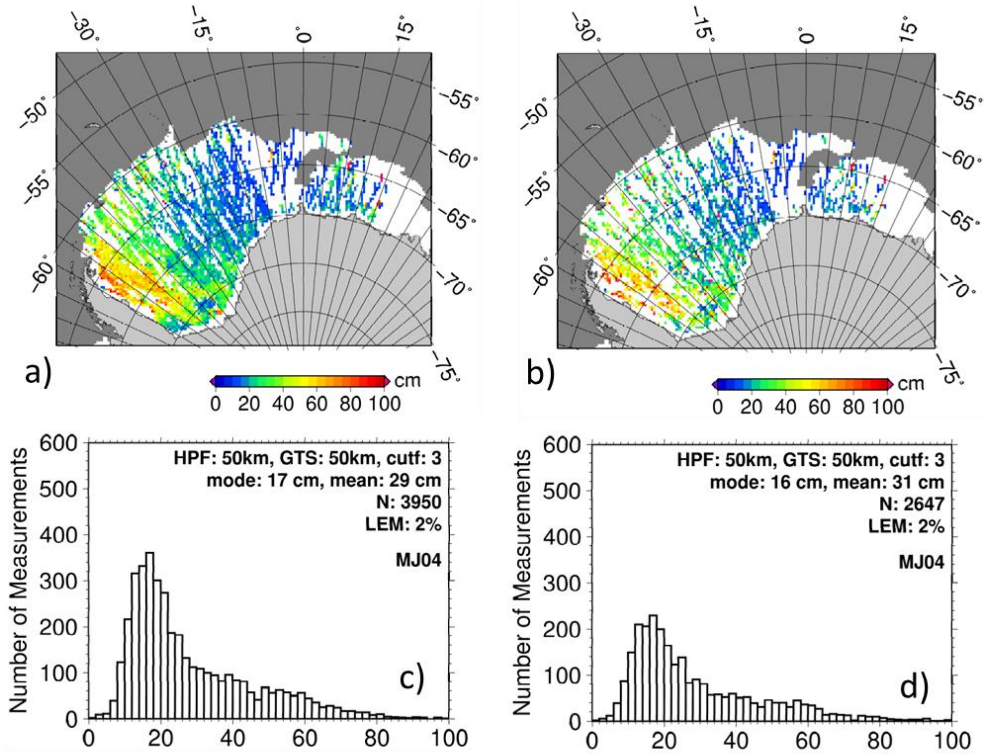

Figure 4.3.3 Freeboard distribution for period May/June 2004 (MJ04) obtained with the SICCI approach (a) and with a modified SICCI approach using only elevation minima with a reflectivity below 0.5 (b); images c) and d) show the corresponding histograms where freeboards are shown with a bin size of 2 cm (x-axis is in cm). White grid cells denote areas with no valid ICESat-1 freeboard data. Grid size is 25 km.

Entire Southern Ocean

The SICCI approach was also used to compute freeboard for the entire Southern Ocean. The results are shown for ICESat-1 measurement periods February/March 2004 to October/November 2007 in Figures 4.3.4 and 4.3.5. This time histograms are shown together with the maps. It is evident from these maps that besides the Weddell Sea regions Ross Sea and Bellingshausen/Amundsen Sea have the best data coverage. East Antarctica is poorly covered by ICESat-1 measurements.

The features known already about sea ice thickness distribution in the Southern Ocean are evident in our results as well: An area of larger freeboard along the coasts of the Bellingshausen and Amundsen Seas which extends into the Ross Sea from the East, a pronounced area of low freeboard in the area downstream of the Ross Ice Shelf polynya, and again relatively large freeboard further to the West between the Ross Sea and the Mertz Glacier. The increase in modal and mean freeboard over the season is confirmed also for the entire Southern Ocean.

The tendency that data coverage is best for the May/June ICESat-1 measurement periods as evident from Figure 4.3.1 is confirmed in Figures 4.3.4 and 4.3.5 as well. Many data gaps occur particularly during the period in late winter/spring.

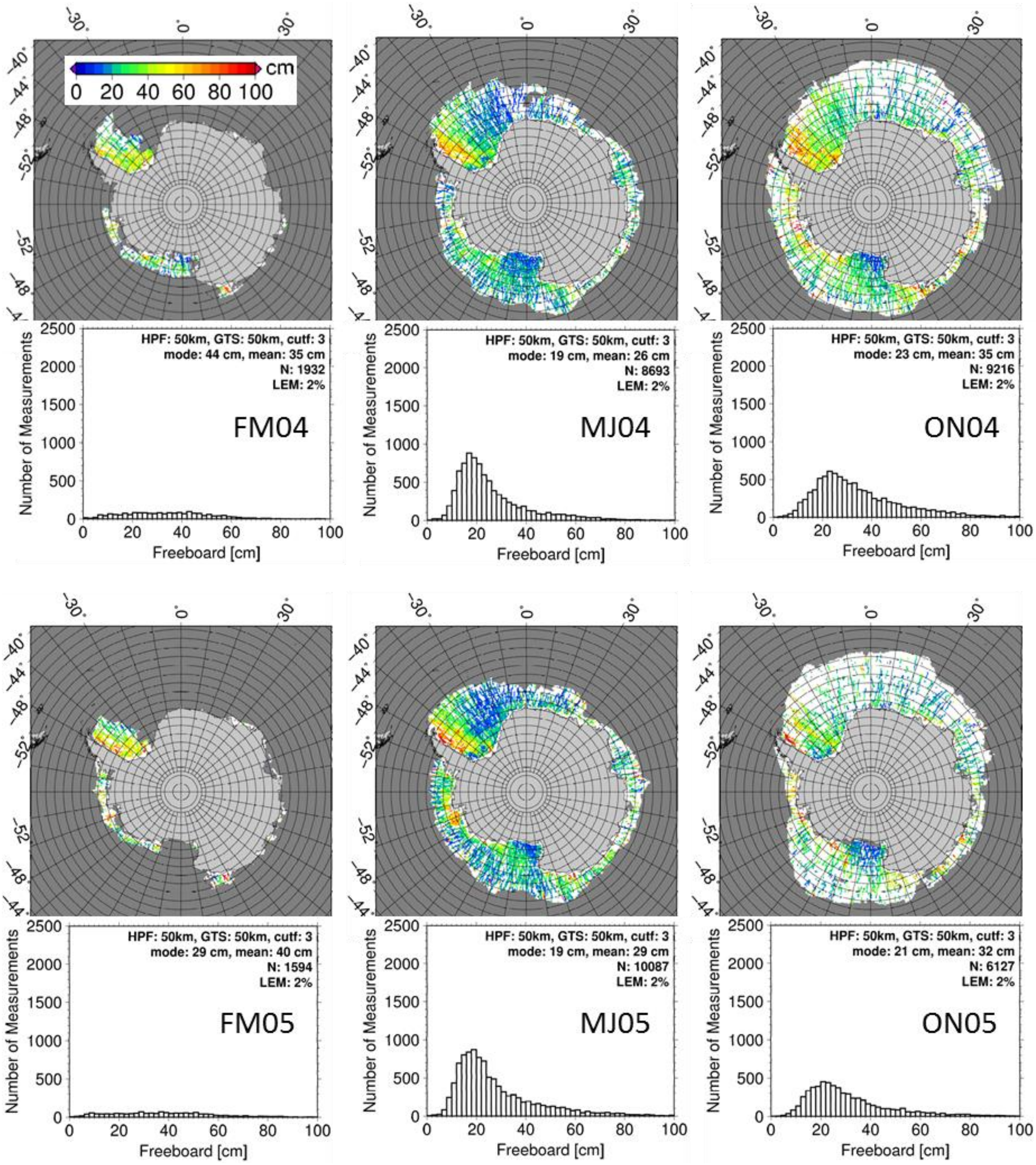

Figure 4.3.4 Freeboard distribution of the entire Southern Ocean as map and corresponding histogram for February/March 2004 to October/November 2005. See also Fig. 4.3.1 and Fig. 4.3.2. White areas denote missing valid ICESat freeboard data.

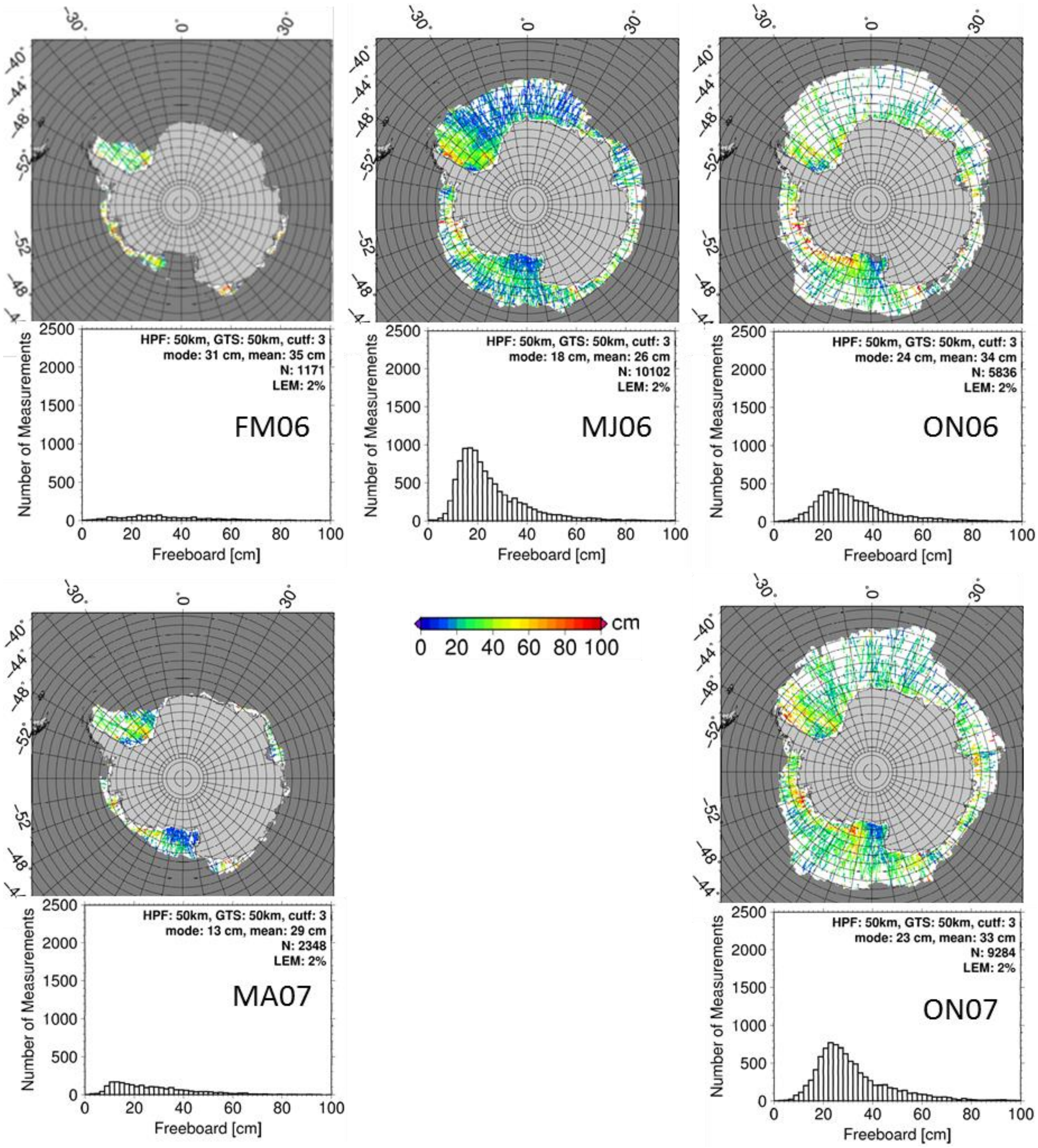

Figure 4.3.5 As Figure 4.3.4 but for February/March 2006 to October/November 2007. Data for February/March 2008 are calculated but not shown for better visibility.

It seems that with the grid cell size used (25 km) data coverage might remain too sparse during later winter/spring periods and also particularly in the East Antarctic region.

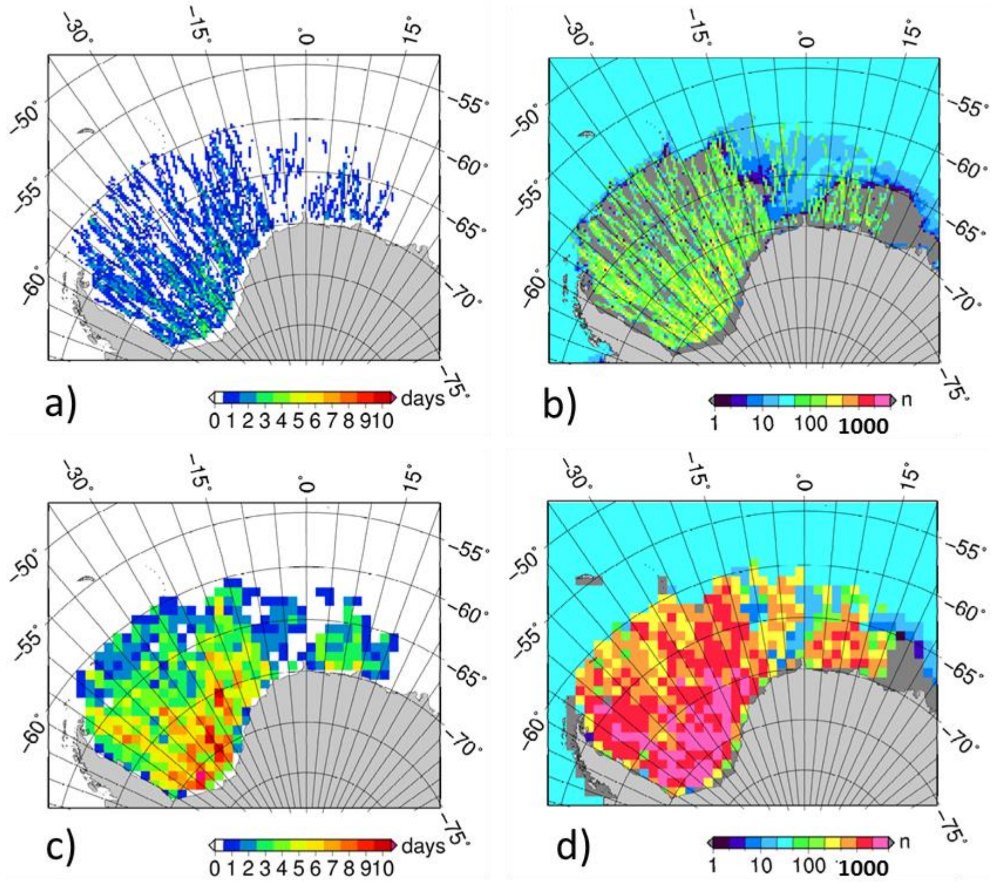

Figure 4.3.6 Number of days for which ICESat-1 measurements contribute to a grid cell mean value for 25 km grid resolution (a) and 100 km grid resolution (c) for the Weddell Sea, period May/June 2004. Number of valid ICESat-1 freeboard measurements per grid cell for the same period for 25 km grid resolution (b) and 100 km grid resolution (d).

There is another thing worth mentioning with regard to the grid cell size used so far. The number of days with ICESat-1 measurements in a particular grid cell is particularly low when using 25 km grid resolution. Usually less than 3 days with ICESat-1 data contribute. With a period length of 33 to 35 days this is less than 10% of the time. If we use 100 km grid resolution the number of days with ICESat-1 data contributing to a grid cell mean value is more than 3-4 days for most of the Weddell Sea; some grid cells might even be based on ICESat-1 data from 8 or more days. This is illustrated in the left hand side of Figure 4.3.6. Associated with this is an increase in the average number of single shot freeboard estimates contributing to one grid cell mean (see Figure 4.3.6 b) and d). Around 100 single measurements contribute to a grid cell mean within one ICESat-1 measurement period at 25 km grid resolution while this number is an order of magnitude larger at 100 km grid resolution. Finally, the number of grid cells with no valid ICESat-1 freeboard data also decreases when using 100 km instead of 25 km grid resolution.

Accordingly, we computed Antarctic freeboard also with 100 km grid resolution. The resulting maps are compiled in Figure 4.3.7. These are quite similar to Figure 4.3.4 and 4.3.5, however, the spatial coverage is much better and the number of data gaps is much smaller.

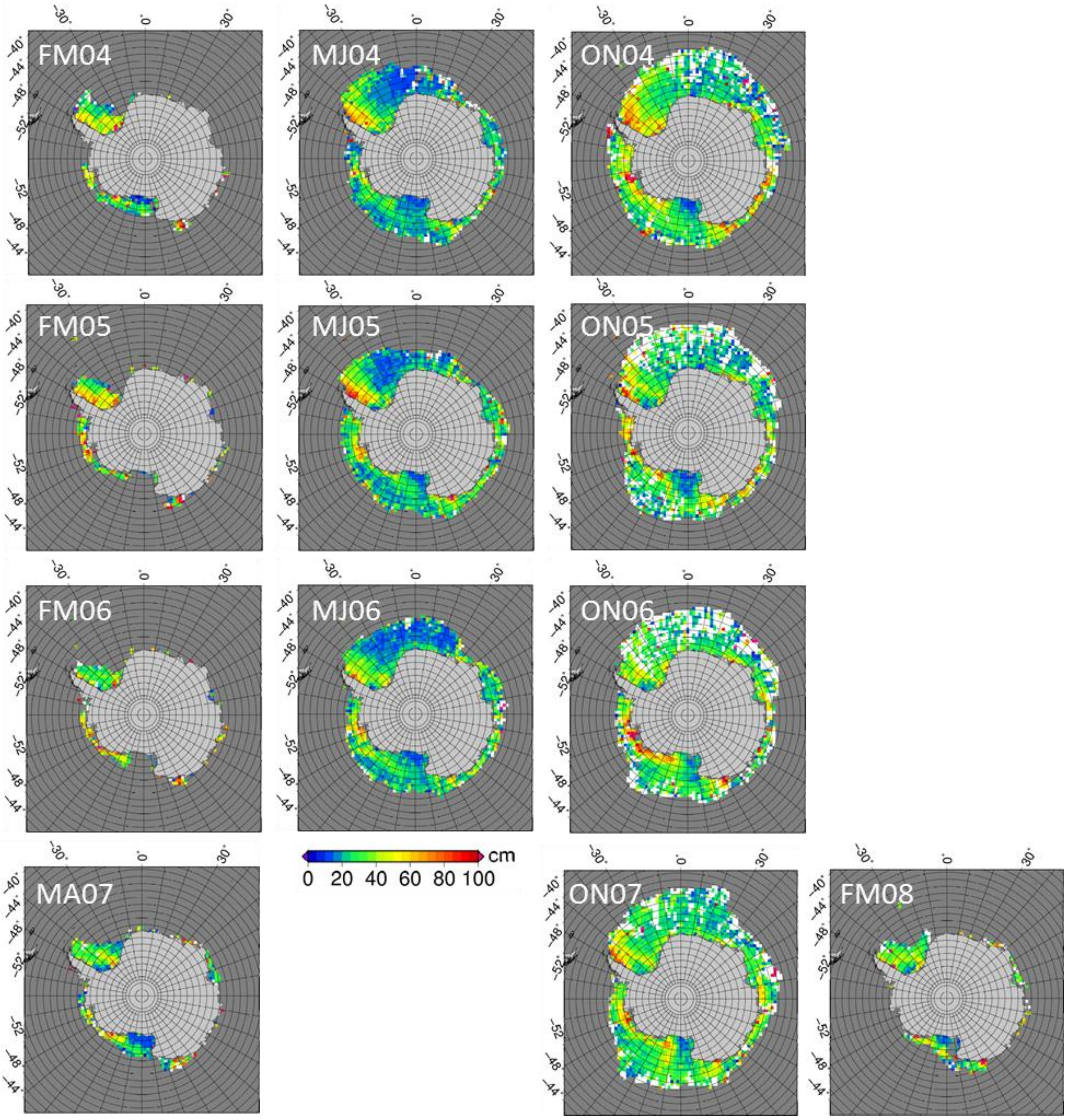

Figure 4.3.7 Freeboard of the Southern Ocean obtained from ICESat-1 for measurement periods February/March 2004 (FM04) to February/March 2008 (FM08) at 100 km grid resolution. White grid cells denote missing valid ICESat-1 freeboard data.

Table 4.3.1 summarizes the mean and modal freeboard values of the entire Southern Ocean for 25 km and 100 km grid resolution. Modal freeboard values are smallest for the May/June (MJ) periods and increase towards late winter/early spring. The inter-annual variation is of the order of a few centimetres during these periods. The same applies to the late winter/early spring (ON) periods. This differs for the fall periods (FM and MA). Here the modal values might be larger than the mean one in contrast to the other two measurement periods. Inter-annual variation for the mean freeboard is within 5-10 cm while modal values vary quite a bit. We note however, that finding the correct modal value is difficult for the sea ice thickness distribution observed during fall (see Figure 4.3.4 and Figure 4.3.5): the histograms are quite wide and do not have a clear mode. Only period MA07 has a clear mode because it is later in the season and hence new ice formation has already resulted in a more extensive thin ice cover than during FM periods.

For the early-to-mid winter (MJ04 to MJ06) and the late winter/early spring (ON04-ON07) measurement periods the difference between the two resolutions is less or equal 2 cm. For the fall periods the difference can be up to 5 cm for the mean freeboard values. This can be explained with the relatively small number of grid cells with valid data during these periods.

Table 4.3.1 Modal and mean freeboard values obtained from ICESat-1 for the Southern Ocean in centimetres. $F_{modal25}$ and $F_{modal100}$ denote the modal values at 25 km and 100 km, respectively; F_{mean25} and $F_{mean100}$ denote the corresponding mean freeboard values.

	FM04	MJ04	ON04	FM05	MJ05	ON05	FM06	MJ06	ON06	MA07	ON07	FM08
$F_{modal25}$	44	19	23	29	19	21	31	18	24	13	23	32
F_{mean25}	35	26	35	40	29	32	35	26	34	29	33	33
$F_{modal100}$	24	19	24	16	21	22	22	18	26	19	23	29
$F_{mean100}$	36	26	35	43	30	33	39	28	35	32	33	38

4.4 Comparison of SICCI freeboard with NASA freeboard and literature

In this section we compare the freeboard obtained with the UH approach (modified from Yi et al. [RD-13] as detailed in Kern and Spreen [RD-23]) with the freeboard obtained using the approach of Markus et al. [RD-14] available from NASA (see section 3.4, [RD-25]). We note that the SICCI algorithm is only modified slightly compared to the algorithm of Yi et al. [RD-13] and therefore for the Weddell Sea freeboard histograms agree well and mean freeboard values agree with those of Yi et al. [RD-13] within 1 cm.

Figure 4.4.1 to 4.4.3 show histograms of the single shot freeboard estimates from the SICCI approach and the NASA data set for fall, winter, and spring ICESat-1 measurement periods, respectively, for the entire Southern Ocean. In fall (Figure 4.4.1) SICCI provides more freeboard estimates in 3 of the 5 years, particularly in 2008. One explanation is that we applied varying gain threshold for the filtering of the ICESat elevation prior to processing as done in Yi et al. [RD-13] while Markus et al. [RD-14] and Kurtz and Markus [RD-15] used a constant gain value. Because the power of the laser instruments aboard ICESat-1 varied over time setting a constant gain threshold is a sub-optimal solution to keep as many valid ICESat-1 elevation measurements as possible. The other explanation is that the way SSH tie points are selected in the approach of Markus et al. [RD-14] potentially discards more values. Apart from that distributions are relatively similar. Modal SICCI freeboard values for 2007 and 2008 are 5 – 10 cm higher than those from the NASA data set. The SICCI freeboard mode for fall is in the 10-15 cm bin except in 2008, where it is in the 15-20 cm bin.

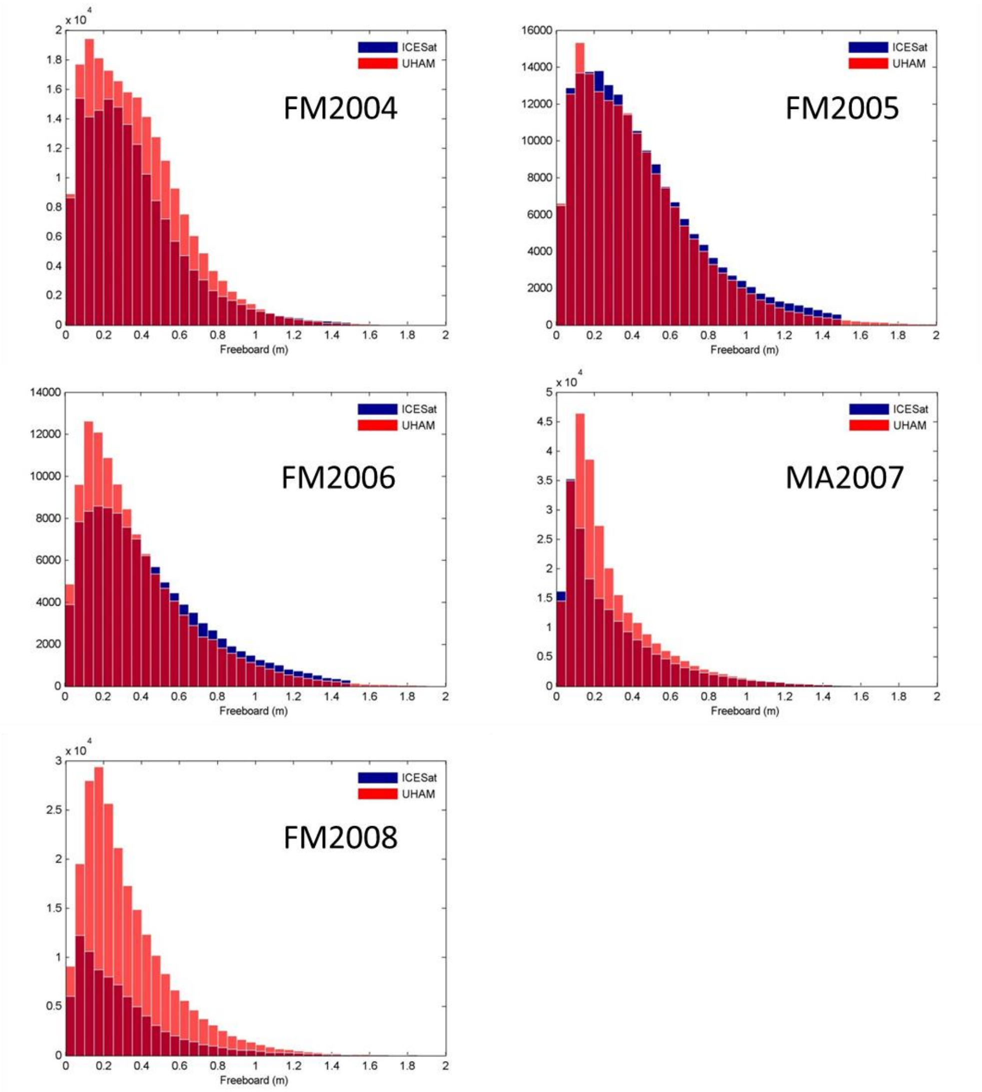

Figure 4.4.1 Single shot freeboard obtained with SICCI algorithm (orange bars) in comparison to single shot freeboard from the NASA data set (blue bars) for fall (February/March) periods. Where the NASA data set overlaps with the SICCI data sets the bars are red-brown. Bin-size is 5 cm, first bin is 0-5 cm, second 5-10 cm, etc.

Figure 4.4.2 confirms the observation of Figure 4.4.1: the shape of the histograms is similar, but SICCI has more values. Most importantly however, modal values are about 5 cm higher for SICCI freeboard than for NASA freeboard. The same is also valid for the spring periods (Figure 4.4.3).

In winter and also in spring the NASA freeboard data sets tends to have more very small (0-15 cm) freeboard values than the SICCI data set. At high freeboard there seem to be no differences between the two data sets.

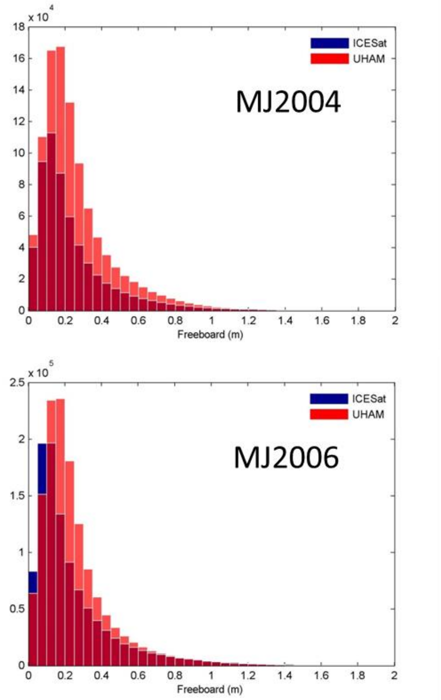

Figure 4.4.2 As Figure 4.4.1 but for winter (May/June) periods.

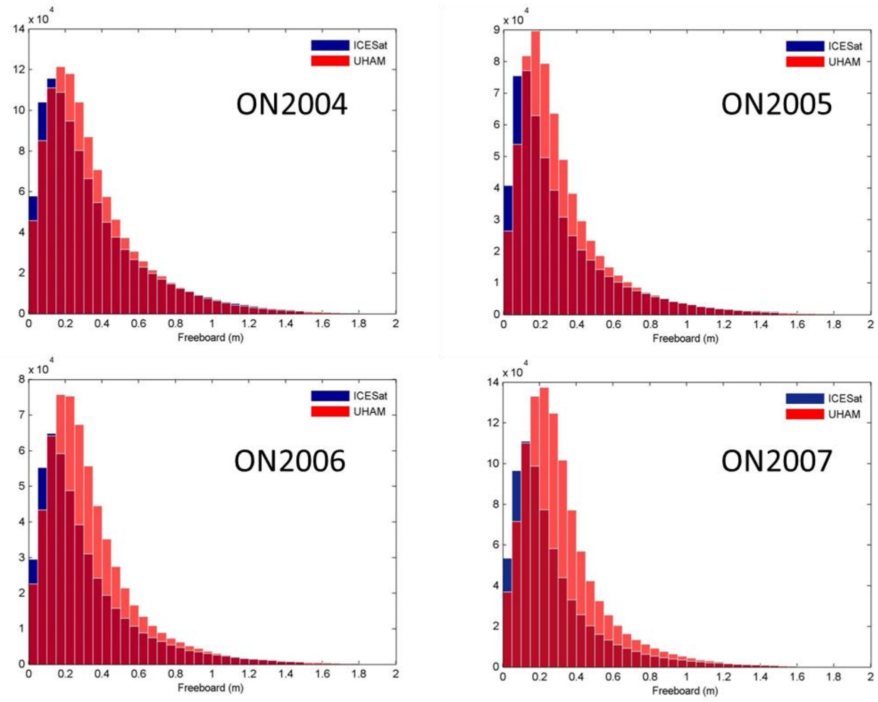

Figure 4.4.3 As Figure 4.3.1 but for spring (October/November) periods.

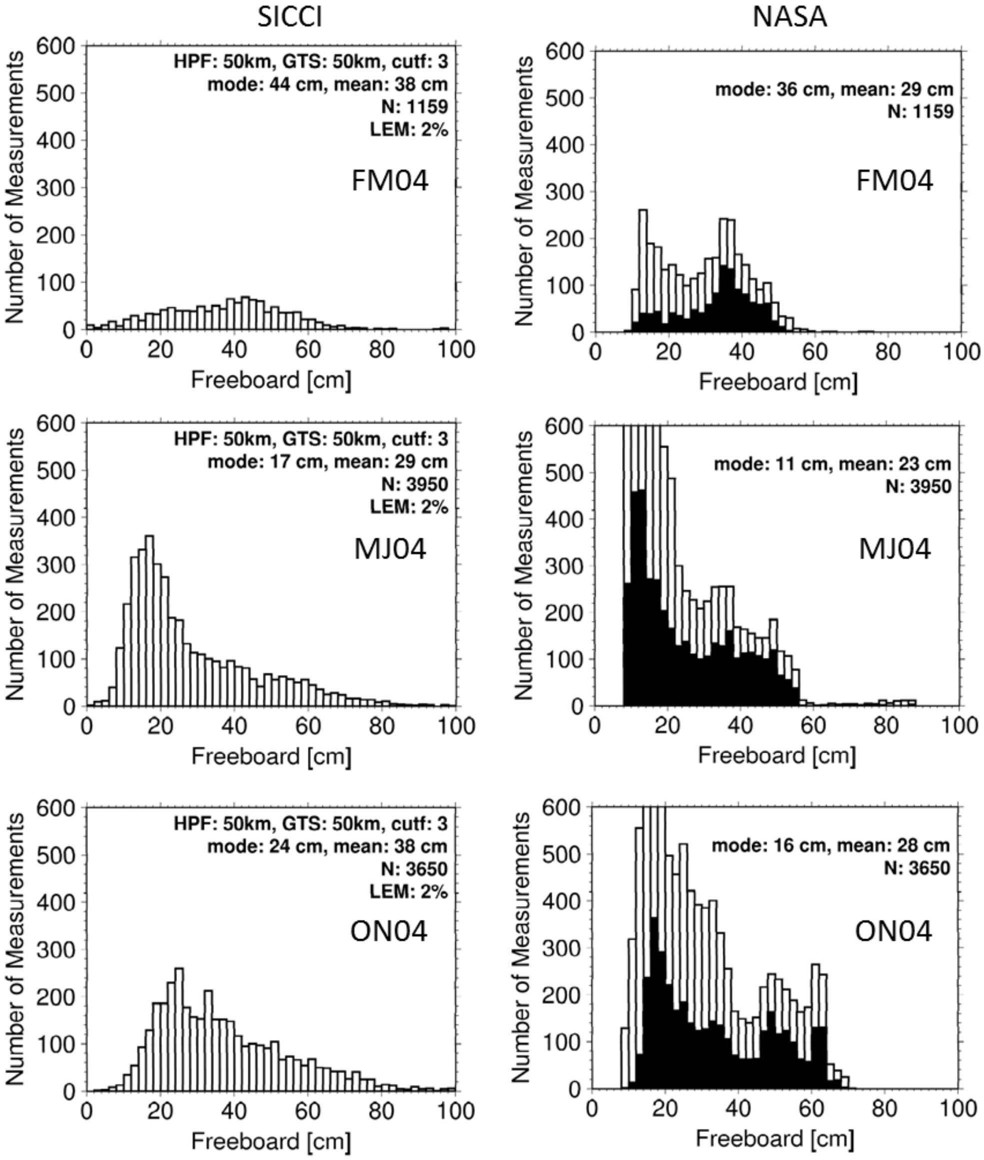

Figure 4.4.4 Comparison of gridded freeboard from SICCI (left) versus NASA (right) for fall, winter, and spring periods (from top to bottom) for the Weddell Sea. NASA freeboard histograms show the entire region as open bars and those collocated with the SICCI freeboard with filled bars. Hence filled bars in the right hand side images compare to the histograms in the left hand side images.

Once the freeboard values are gridded onto a polar-stereographic grid with 25 km grid resolution maps like those shown in Figure 4.3.1 are obtained. We compared SICCI ICESat-1 freeboard data (Figure 4.3.1) with the respective values in the NASA freeboard data set. We used only grid cells which have valid SICCI ICESat-1 freeboard measurements. The histograms of these collocated freeboard data sets are shown in Figure 4.4.4. It is clearly evident that the distribution, the modal values and the mean values differ substantially between both data sets. In particular the gridded NASA ICESat-1 freeboard data set seems to have cut off low freeboard values and high freeboard values. The NASA freeboard mode and mean are between 6 and 8 cm and 6 and 10 cm smaller than respective SICCI freeboard values. We would assume in view of other literature reporting on gridded ICESat-1 freeboard in the Antarctic [RD-12; RD-13] that the SICCI results look more realistic at the lower and higher end of the freeboard distribution. Whether in general SICCI or NASA freeboard values are better we cannot say without inter-comparison with independent freeboard estimates which are not available.

We note that one reason for the discrepancy between the SICCI and the NASA gridded ICESat-1 freeboard data sets could be the gridding procedure used. While SICCI uses drop-into-the-bucket without interpolating between ICESat-1 tracks NASA uses kriging interpolation to fill gaps between the tracks. It is likely that this also influences the original values and smoothes the freeboard distribution in general.

4.5 Uncertainties

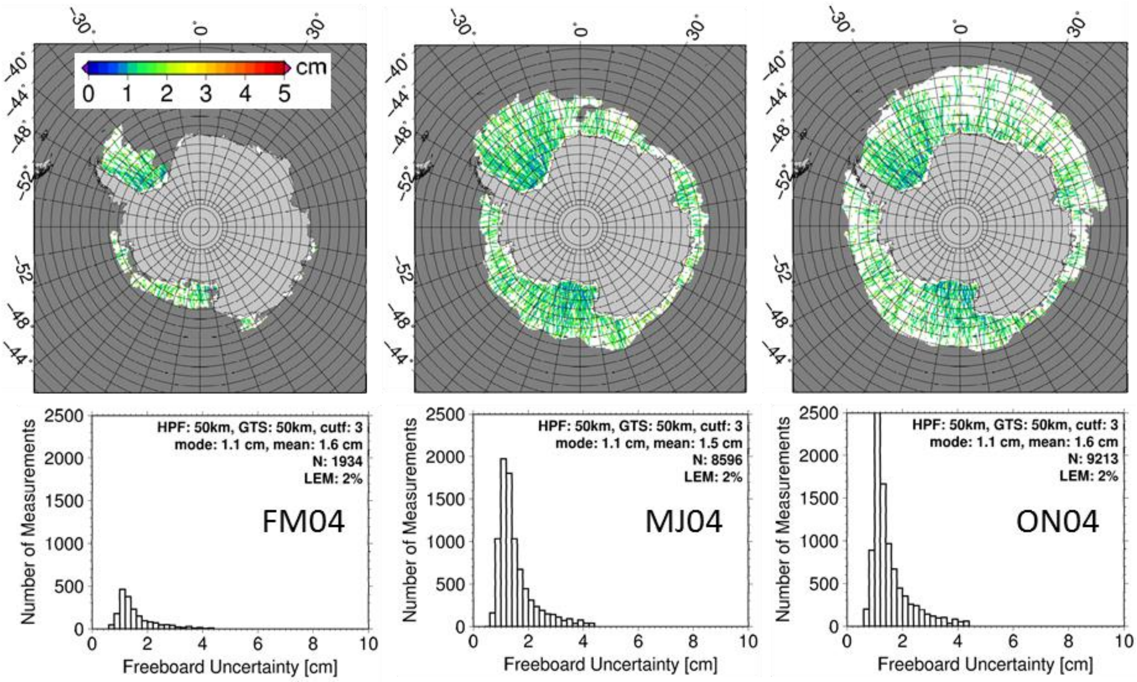

Figure 4.5.1 Gridded single laser shot uncertainty for fall, winter, and spring ICESat-1 measurement period in 2004. Grid resolution is 25 km. White areas denote regions with no valid ICESat-1 freeboard data.

In section 3.6 we wrote about the uncertainty estimation of ICESat-1 freeboard data and explained that due to the lack of contemporary data it is difficult to get a quantitative uncertainty estimate. One contribution to the gridded ICESat-1 freeboard uncertainty estimate is the average single laser shot uncertainty. This is shown for ICESat-1 measurement periods of the year 2004 in Figure 4.5.1. Because the single laser shot uncertainty is constant this gridded uncertainty is basically a function of the number of valid measurements per grid cell. This explains why the maximum uncertainty shown in the histograms of Figure 4.5.1 does not exceed 4.3 cm and why the modal value of the gridded uncertainty takes a value of 1.1 cm for all three periods shown (and also for the other periods not shown); the modal number of measurements within a 25 km grid cell is about 155. We note that the gridded uncertainty reduces for 100 km grid resolution because more valid measurements are used; the modal gridded uncertainty takes a value of about 0.6 cm in this case.

These uncertainty values are considerably smaller than the 2 to 4 cm suggested from ICESat-1 data analysis in the Arctic (see Section 3.6). The results of the sensitivity analysis (see Sections 4.1 and 4.2) reveal that choosing input parameters to the lowest level elevation method (LLEM) which are not fitting the environmental conditions can easily cause basin wide biases of the order of 2 cm to 5 cm; regionally biases can even exceed 10 cm. An optimal choice of these input parameters cannot be guaranteed and/or would require additional data to be used, such as lead concentration or sea ice concentrations which are as accurate as 1-2% at the high concentration range – a yet impossible to fulfil requirement. Also the association of the above-mentioned uncertainties derived with the sensitivity study would require such independent information. Because such additional information is not available our recommendation is to use the gridded single laser shot uncertainty multiplied by a factor of 3. This is a somewhat arbitrarily chosen factor but it has two advantages. First it brings the freeboard uncertainty estimate to be used for sea ice thickness retrieval uncertainty estimation to a level which is compliant with the results of the sensitivity study. Secondly it includes the dependency of the quality of a gridded ICESat-1 freeboard value to the number of single ICESat-1 measurements.

4.6 Outlook

As detailed above further refinement of the freeboard retrieval is difficult without contemporary independent data. What can and should be done, however, is the improvement of the uncertainty estimation.

The choice of percentage P used for the SSH tie point selection is a function of the lead concentration and/or open water fraction along the ICESat-1 track. A natural next step would be therefore to combine the ICESat-1 data with information about lead concentration as has been derived for the Arctic from, e.g., Advanced Microwave Scanning Radiometer (AMSR-E) data [RD-36]. Such data could not only help for the uncertainty estimation but also for the freeboard retrieval itself.

Another way to estimate uncertainties is cross-track analysis. The difference in the freeboards derived from ICESat-1 tracks crossing each other could be taken as an uncertainty estimate. This requires however that the cross-over points are located in regions where the ice drift over the time period used for the cross-over analysis is negligible. Obvious regions for this would be fast ice. However, ICESat-1 elevation measurements of the ICESat-1 product used in the SICCI project may start at some distance to the coast, depending on the orientation of the ICESat-1 track to the coastline (see e.g. Figure 4.2.1). Hence the number of elevation measurements over fast ice could be limited to only a few locations.

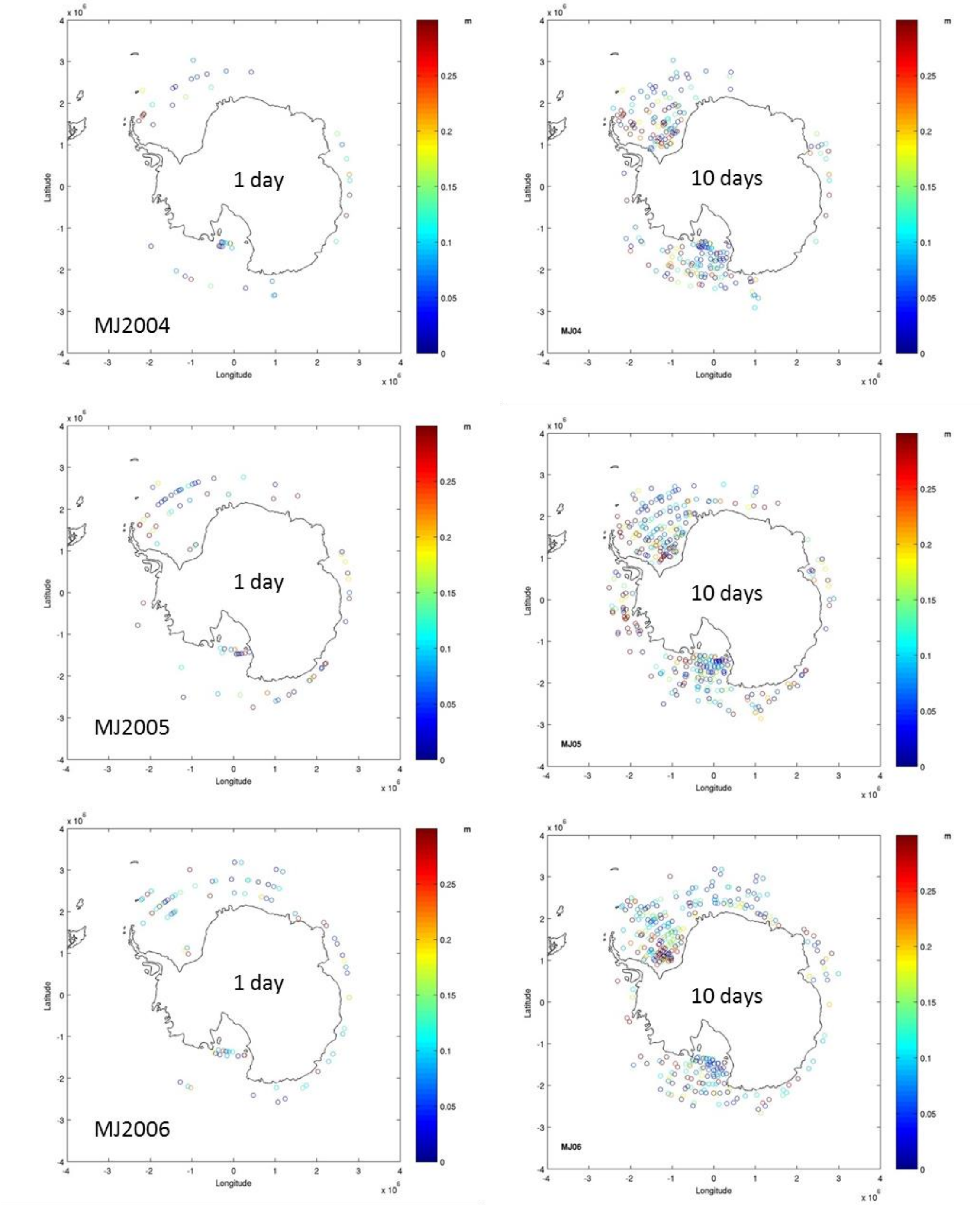

Figure 4.6.1 Cross-over points found for the three winter ICESat-1 measurement periods using a maximum time difference of 1 day (left) and 10 days (right).

Figure 4.6.1 illustrates that for winter periods (May/June) the number of cross-over points increases substantially from using a 1-day threshold to a 10-day threshold. The locations of most cross-over points are, however, clearly in drift ice regions in the images on the right hand side. The same applies – unfortunately – also for the 1-day cases (left hand side). The Ross

Ice Shelf polynya area shows quite a large number of cross-over points. Even though this could be a region of substantial ice drift, the renewal of the sea ice at a certain distance from the shelf due to the frequent ice production in the polynya might support ice conditions which have a higher probability for a rather constant freeboard within 1 day time difference while sea ice in other regions more likely is a mixture of thick and thin drift ice.

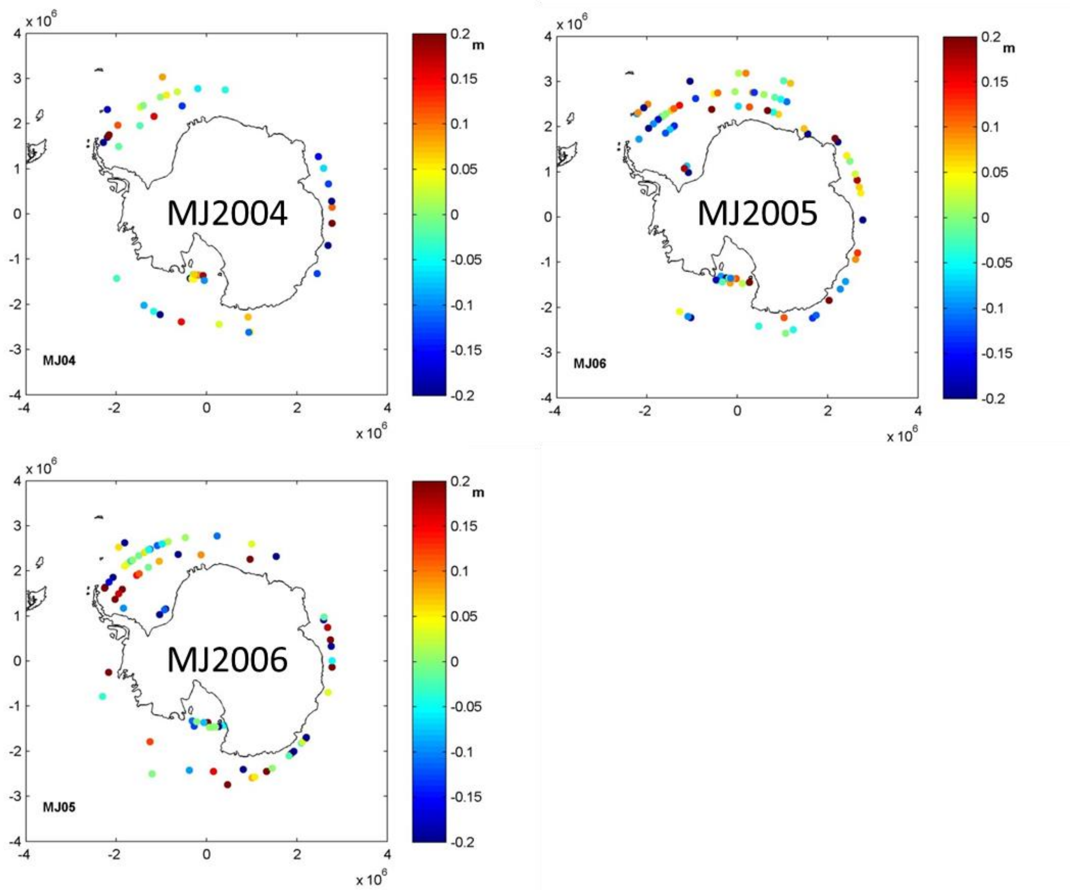

Figure 4.6.2 Freeboard difference (in m) at cross-over points using the 1-day threshold

Figure 4.6.2 illustrates the distribution of freeboard differences at the ICESat- track cross-over locations shown in Figure 4.6.1, left hand side. Ideally we would have expected to see many green dots with freeboard differences in the range -5 cm to +5 cm. However, neither in the Ross Ice Shelf polynya area nor in the other areas the difference seems to fall into this range. We note, however, that we are talking about a 60 m footprint and an inter-footprint distance of 172 m. Given the natural variability of a sea ice cover it is more than likely that within a day ice of a different thickness and/or snow depth and hence different total freeboard has replaced the sea ice sensed at the first day.

Figure 4.6.3 shows the histograms of the freeboard differences shown in Figure 4.6.2 for the SICCI approach (denoted “UHAM”) as well as the NASA data set (denoted by “ICESAT”) (see Section 4.4). This figure shows that freeboard differences are basically symmetric around zero. Also, about 90% of the absolute freeboard differences are smaller than 0.2 m. More investigations are needed to figure out whether such an analysis is going to help with a better quantification of the freeboard uncertainties. One idea would be to find contemporary information about fast ice location and extent.

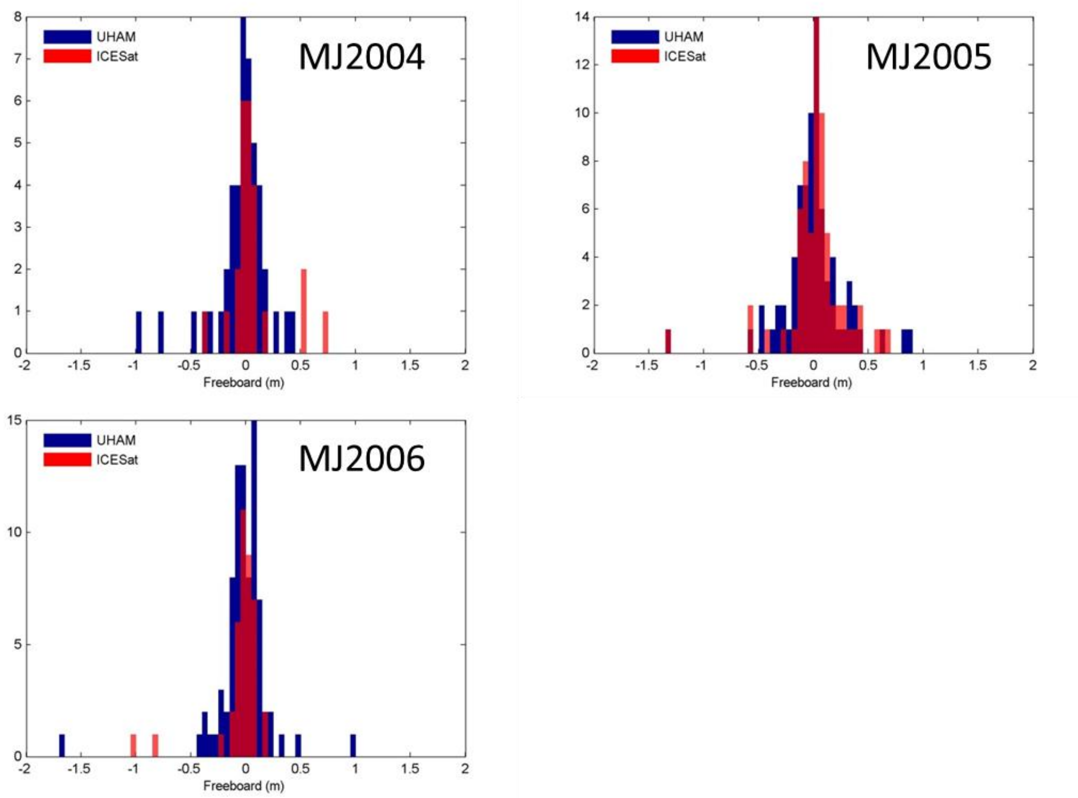

Figure 4.6.3 Histograms of the freeboard differences shown in Figure 4.6.2 (denoted "UHAM", in blue). In addition freeboard differences obtained from the NASA freeboard data set (denoted "ICESAT", in orange) are displayed. Where both data sets overlap bars are brown. Bin size is 0.05 m.

Finally, it is shown that using a 100 km grid provides a better spatial coverage of the Southern Ocean with valid ICESat-1 freeboard data. In order to figure out a grid resolution which accounts optimally for the typical scale of spatial freeboard variations an auto-correlation analysis could be carried out with long single ICESat-1 tracks. This is work in progress and might be reported together with results of the other two issues mentioned in this section, i.e. usage of lead concentration and cross-over analysis, in an update of this report.

5 Freeboard retrieval of Antarctic sea ice using ICESat: Summary

Freeboard retrieval using ICESat-1 elevation measurements in the Antarctic is in general possible and works sufficiently well for the entire Southern Ocean and all ICESat-1 measurement periods.

The main difficulty with the assessment of ICESat-1 freeboard is the lack of contemporary independent freeboard estimates. Antarctic ICESat-1 freeboard cannot be validated as it has been done in the Arctic.

A comparison to sea ice freeboard obtained from Envisat radar altimetry will be given in deliverable D1.4. A comparison to snow depth on sea ice estimates will be given in deliverable D1.2. Both may serve as a consistency check of the ICESat-1 freeboard – provided that the data used for the consistency check are valid.

The so-called lowest level elevation method (LLEM) used by various authors provides realistic estimates of the freeboard and its distribution around Antarctica. Attention needs to be paid to the different ways the LLEM is used because differences in the freeboard obtained with two different methods could translate into differences in mean sea ice thickness obtained of 50 cm or more. We recommend using the LLEM as it has been proposed first by Zwally et al. [RD-12], refined by Yi et al. [RD-13] and modified slightly in Kern and Spreen [RD-23].

A sensitivity analysis of input parameters for the LLEM suggest that the gridded freeboard uncertainty is larger than values obtained for the Arctic and it is larger than the gridded single laser shot uncertainty. To estimate sea ice thickness uncertainty based on ICESat-1 we recommend to multiply the gridded single laser shot uncertainty by a factor of 3. We note that uncertainties can be expected to be higher in areas of compact sea ice with a below-average number of leads and in areas influenced by ocean swell.

Usefulness of ICESat-1 freeboard retrieval for the estimation of an Antarctic wide sea ice thickness is limited by i) the limited coverage in time, which is only up to three about 35 days long periods per year between 2003 and 2009, and by ii) the limited coverage in space caused by the need to filter out data with, e.g., too low signal strength (gain filter), pronounced forward scattering, or saturated waveforms.

Our results indicate that a careful gridding of the ICESat-1 single shot freeboard measurements is required. Different gridding methods, interpolation or even extrapolation might result in dubious freeboard distributions over space and the freeboard value range.

Still ICESat-1 freeboard data can serve as an important base to obtain freeboard estimates during up to 3 important time periods in the Antarctic seasonal sea ice thickness cycle.

< End of Document >